Lamessa et al. Geoenvironmental Disasters (2019) 6:16
https://doi.org/10.1186/s40677-019-0131-y

Geoenvironmental Disasters

RESEARCH Open Access

Homogenized earthquake catalog and b-value mapping for Ethiopia and its adjoining regions

Geremew Lamessa*, Tilahun Mammo and Tarun K.Raghuvanshi

Abstract

The Ethiopian rift which is part of East African Rift system passes through the middle of the country making it one of the most seismically active regions in the world. Thus, significant and damaging earthquakes have been reported and recorded in the past in this region. A homogeneous earthquake catalog is of basic importance for studying the earthquake occurrence pattern in space and time and for many engineering applications including assessment of seismic hazard, estimation of peak ground accelerations and determination of long-term seismic strain rates.

The first earthquake catalogue for Ethiopia was prepared by Pierre Gouin and later, different authors attempted to compile a catalogue using different time period intervals and different earthquake magnitude scales. The b-value mapping and its implication never done for Ethiopia and its environs. The main purpose of the study is therefore first compile and homogenize earthquake catalog of Ethiopia including Read Sea and Gulf of Aden regions into Moment magnitude Mw scale through completeness analysis in time and magnitudes. Secondly, mapping b-values for different Seismgenic regions and understand its implications for magma induced Seismicity in the regions.

During the present study, a new homogenized earthquake catalog in moment magnitude scale (Mw), covering about 3814 events is prepared for Ethiopia including Red sea and Gulf of Aden regions. The present study area is bounded within Latitude (4^0N – 20^0)N and Longitude (34^0N – 48^0)N E and have a magnitude range of Mw (3.0–7.1) with a total coverage period of 56 years (1960 to 2016). The catalog has been analyzed for magnitude completeness (Mc) using Gutenberg's Frequency Magnitude Distribution law and it is found to be complete respectively for Mc ≥ 4.6 ± 0.03, Mc ≥ 4.6 ± 0.03, Mc ≥ 3.2, Mc ≥ 3.1 and Mc ≥ 5.1 for Afar including red sea and Gulf of Aden, Afar rift and Dabbahu Volcano, Northern, Central, and Southern Main Ethiopian Rifts. Further, the corresponding average b-value of the regions Afar including Red Sea and Gulf of Aden, Afar and Dabbahu Volcano separately, Northern Main Ethiopian Rift, Central Main Ethiopian Rift and Southern Main Ethiopian Rift respectively are estimated to be 1.17 ± 0.05, 1.15 ± 0.05, 0.843, 0.826 and 1.03 with respective period of completeness from 2003 to 2014, 2005 to 2014, 2001 to 2003, 2001 to 2003 and 1960 to 2016 for the regions. Later, mapping of the b-values in the Gutenberg-Richter relation from the newly developed catalog was performed by binning the regions into minimum of 0.05^0x0.05^0 for Afar and Dabbahu region, 0.1^0x0.1^0 for Main Ethiopian rifts and 0.2^0x0.2^0 for the other regions. Thus, the b-value characteristics of various seismogenic zones within the area have been discussed. Hence, in this study, we clearly observed that magma chamber movement including mapping of volcanic centers and magmatic segments are mapped using b-values.

Keywords: Earthquake catalog, Magnitude of completeness, b-values, Magmatic segments

* Correspondence: olbirat2010@gmail.com
Addis Ababa University, School of Earth Science, Addis Ababa, Ethiopia

Introduction

The Ethiopian rift System which is part of East African Rift system passes through the middle of the country making it one of the most seismically active regions in the world. Thus, significant and damaging earthquakes have been reported and recorded in the past in this region. Of these, the 1906 Langano earthquake with magnitude 6.8 (mb), the 1961 Kara Kore earthquake magnitude 6.4(mb) which caused damage to manmade structures (destroyed the town of Majete) and alterations in the landscape, and the 1969 Serdo earthquake magnitude 6.5(mb) are significant ones (Kebede 1996).

For understanding of Seismicity of a region, the knowledge of the geological history and detailed interpretation of the resulting structure are important. Studies indicated that the result of geodynamic and geomorphic processes shaped Ethiopian territory since the Oligocene (Abbate et al. 2015). These processes were activated by the impingement of plumes under the Afro- Arabian continental crust. The plume action contributed the rise to extrusion of huge amounts of magma, uplift, and fragmentation of the continental crust and contributed to the birth of the Red Sea, Gulf of Aden, East Africa Rift valley, and the adjoining Afar depression.

The accommodating laboratory for understanding inactive brim processes, continental disintegration, and the first stages of oceanization is the Eastern Africa Rift in general and the Afar region, as an contestant for the formation of a new oceanic crust in particular (Barberi and Varet 1977; Abbate et al. 2015 and reference therein).

According to Bonini (2005), the East African Rift System (EARS) is a region of continental breakup marking the incipient plate boundary between Nubia and Somalia plates from Djibouti to Mozambique. In the EARS, the Main Ethiopian Rift denotes the connection region between the Afar triple junction and the Kenya Rift regions where extensional deformation nucleated as early as late Oligocene-early Miocene times (Ghebreab 1998; Bellahsen et al. 2003; Morley et al. 2007). EARS' has a complex structural pattern consisting of rift segments with time-space tectonic evolutions that are apparently different one from each other. Three main physiographic provinces characterize the Ethiopian region: the highlands, represented by the Ethiopian and Somali plateaus, Afar depression and the MER (Fig. 1).

The Ethiopian Rift extends for about 1000 km in a NE–SW to N–S direction from the Afar depression, at the Red Sea–Gulf of Aden junction, southwards to the Turkana depression (Corti 2009) accompanied by serious of boarder faults and volcanoes along the rift (Fig. 1).

The seismically and volcanically active main Ethiopian rift is one of few places worldwide where rift evolution from broadly distributed to focused strain can be tracked (Ebinger and Casey 2001).

As built up environments, Engineering structures, and human development activities increase in areas close to and within the Ethiopian rift System, it is expected that the damage on property and loss of human life due to seismic hazard will increase very significantly (Samuel Kinde et al. 2011). Further, the largest and most expensive infrastructure projects are in the seismically active prone regions in the country.

Several magnitude scales are used in earthquake catalogues compiled by seismological centers all over the world to give a measure of the "size" of the earthquakes for better analysis of seismic Hazard. However, these scales do not behave uniformly for all magnitude ranges. Another defect is that the Ms., mb, M_D and M_L scales exhibit saturation effects at different levels for large earthquakes. Both these limitations could result in under- or over-estimation of the earthquake magnitudes and therefore, Kanamori (1974); Hanks and Kanamori (1979) proposed the moment magnitude scale, M_W, directly connecting the seismic moment with the earthquake magnitude, resulting in a uniform behavior for all magnitude ranges. This definition turns M_W into the most reliable magnitude accurately describing the size of the earthquakes. Due to the advantages of the Mw magnitude scale, it is preferred to compile earthquake catalogs with all magnitudes expressed in this unified scale M_w for the purpose of seismic hazard assessment and other important seismological problems having engineering applications (Das and Sharma 2011).

Besides, one of the basic seismological parameters used to describe an ensemble of earthquakes is the b-value in the Gutenberg-Richter frequency-magnitude relation which demands the Homogenized earthquake catalog in moment magnitude scale. In addition, b-values beneath volcanoes have been investigated by numerous scientists. Various studies conducted by Wiemer and Benoit (1996), Wiemer and Wyss (1997), Wyss et al. (2001), Murru et al. (2007) and Cauzzi et al. (2016) came to the conclusion that b-values is promising method to spatially map or model magma chambers beneath the volcanoes. Meanwhile, it is accepted among scientists that elevated b-values in the proximity of a volcano can be used to model the magma chamber.

Furthermore, Complete and Homogenized earthquake catalogues are necessary for the study of earthquake behavior, b-value mapping, designing earthquake resistant structures and understanding geodynamic process associated with earthquakes (Talukdar 2014).

Historical and even instrumental data records are by their nature are incomplete due to lack of earthquake recording instruments during early days of earthquake occurrence and sparse distribution of the instruments in later time (Das and Sharma 2011). Besides, Gutdeutsch

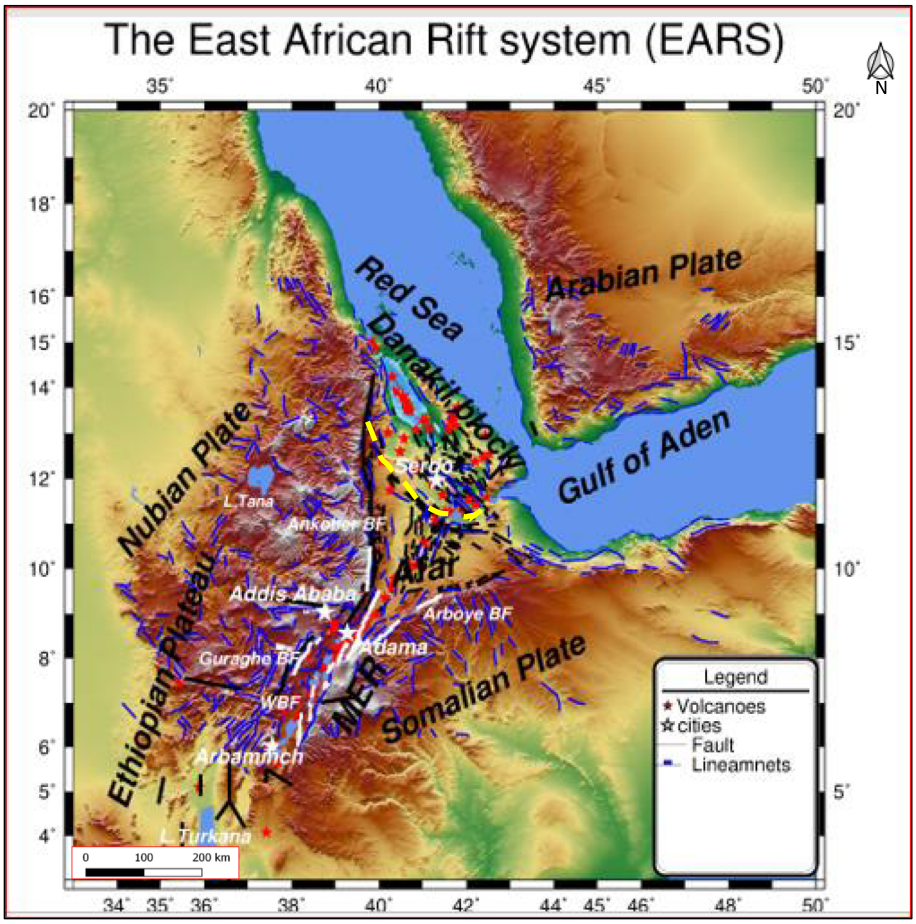

Fig. 1 Tectonic setting of the study region; Colored and shaded relief map of some parts of East African Rift system. Red triangles show volcanoes from the Global Volcanism Program (2013). The East African Rift system separates the Nubian and Somalian plates to the west and east of the rift, respectively. The Arabian plate is separating from Nubia and Somalia with the triple junction at Afar region. The yellow doted curved line indicates the Tendaho-Goba'ad Discontinuity. The black lines indicate Normal and Boarder faults. WBF-Wonji Fault Belt, BF- Boarder Faults

and Hammerl (1999) discussed the reasons for incomplete historical earthquake data.

The first earthquake catalogue for Ethiopia was prepared by Pierre Gouin (1979). Later, Ayele (1995) attempted to compile a catalogue from 1960 to 1993 for the Horn of African region by using body wave magnitude. Both catalogues have used variety of earthquake magnitude scales particularly the latter one was in body wave magnitude scale that makes it difficult to use them for any reliable seismic hazard assessment studies. However, the present study compiles different events of various magnitude scales in one homogenized catalog, expressed in terms of one standard scale, i.e. moment magnitude, M_W. Therefore, the purpose of the present study was firstly to prepare unified Earthquake catalog for Ethiopia and hence generate improved earthquake Catalog for the country through analysis of its completeness (in time and Magnitude). Secondly, present study also focused on computing and mapping of b-Values for the rifts of Ethiopia; Afar rift (including Red Sea and Gulf of Aden), Afar rift and Dabbahu Volcano separately, Northern Main Ethiopian Rift (NMER), Central Main Ethiopian Rift (CMER), Southern Main Ethiopian Rift (SMER) (Fig. 2) and from homogenized catalog moment magnitude Mw. Present study attempts to combine spatial and temporal variations in b-value. The combination of both results might be another tool which seismologists could use to monitor volcanoes and Earthquakes.

Methodology

Seismic data sources

Parametric Earthquake data of Ethiopia and its adjoining regions was compiled in the range of (4^0–18^0) Lat and (34^0–48^0) Lon for magnitude range 3–7, depth 0-60 km, magnitude type -mb, ms, Mw, M_L, M_D. For present study about 7000 Earthquake events of the country and its environs were compiled from 1900 to 2016 (116 years).

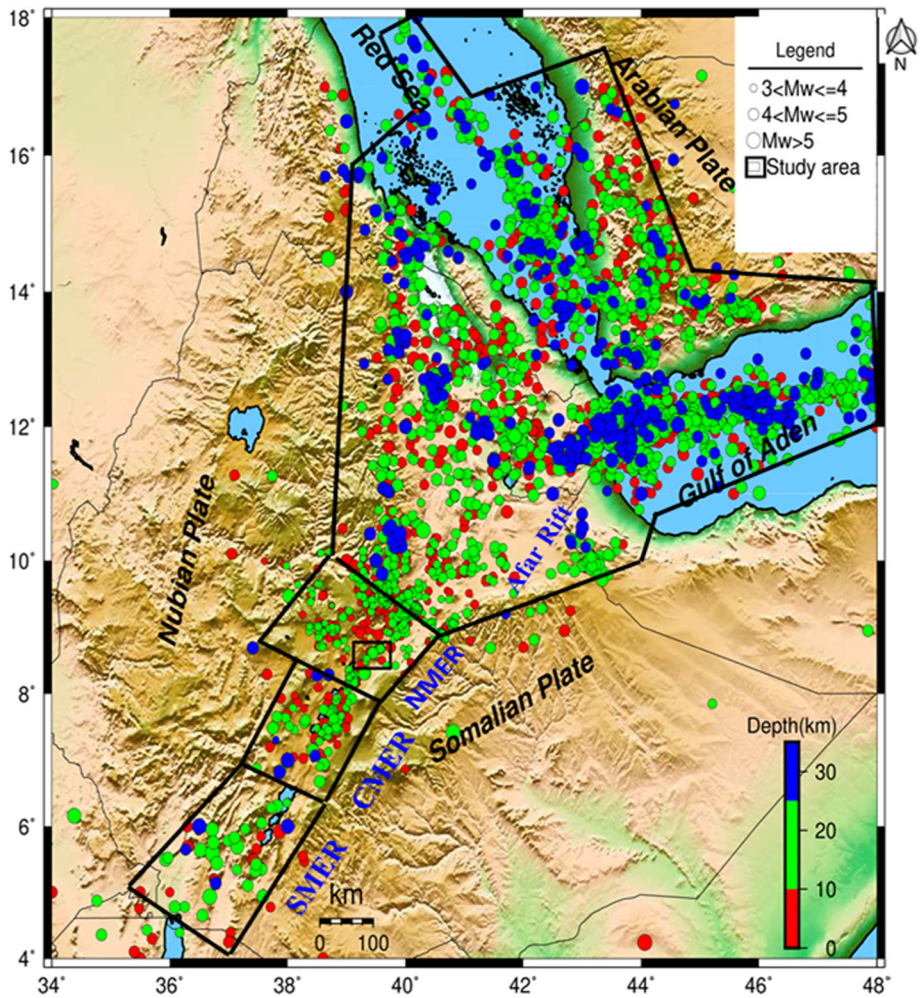

Fig. 2 Seismicity Map of Ethiopian Rifts (Including Red Sea and Gulf of Aden rifts) from the new catalog. The legend color bar on the right bottom of the map indicates the Hypocenteral depths variations of Earthquake. The rectangular legend on the top right of the map indicates the size of the of the Earthquakes magnitude's ranges in Moment magnitude scale in the regions

The earthquake information gathered for each event in the database consists of the earthquake date, epicentral coordinates, earthquake magnitude in various scales moment magnitude (Mw)-very few, surface-wave magnitude (M_s), body-wave magnitude (m_b), duration magnitude (M_D), and local magnitude (M_L)) and depth. In order to compile the earthquake data for a new seismic catalogue of Ethiopia, all the accessible national and international seismological data banks were used. There are some sources of data utilized from works done by Gouin (1970, 1979); Ayele (1995); Kebede (1996); Kebede and Asfaw (1996); Ayele and Kulhánek (1997); Keir (2006); Ayele et al. (2007) on historic and instrumental earthquakes of Ethiopia and its environs.

Furthermore, the instrumental data were compiled from Institute of Geophysics Space Science and Astronomy (IGSSA), Addis Ababa University, International Seismological Centre (ISC)-the ISC Bulletin (Data retrieved from the ISC web site 2015) contains data from 1900 to the present day, National Earthquake Information Center (NEIC)- recorded earthquakes from 1973 to the present, EHB, Bob Engdahl- EHB Bulletin (Data retrieved from the ISC web site 2015) conatains data available for the period 1960 to 2006, and Global Centroid Moment Tensor Catalog (GCMT) (Online data from 1976 up to the present.

Later, all necessary corrections and catalog completeness check has been made, a homogenous Earthquake catalog of Ethiopia and the adjoining regions has been prepared. There after the b-values and b-value maps for respective regions have been computed and prepared respectively. Besides, declustering has been applied to remove fore shock and after shock events to prepare the new homogenized catalog. Hence, Reasenberg (1985) declustering algorithm was used which has been very popular among the seismological communities. Even, Stiphout et al., (2012) and Wiemer (2001) have

considered only the algorithm of Reasenberg (1985) in the latest Zmap of Seismicity analysis. Even though the old version of the Zmap considers Reasenberg (1985) and Gardner and Knopoff (1974) including others declustering algorism like Uhrhammer (1986). The latest Zmap version for Seismicity analysis considers Reasenberg (1985).

Estimating moment magnitude mw from magnitudes (m_b, M_S, M_D and M_L) scales

The earthquake magnitudes were previously reported in different magnitude scales namely; body wave magnitude mb, surface wave magnitude Ms., local magnitude ML and Duration magnitude MD. In the present study moment magnitude scale Mw has been derived by regression relations after performing all necessary corrections and by making all relevant catalog check.

Scordilis (2006) checked that m_b and M_S as reported by ISC were found to be equivalent to mb and M_s of NEIC with the help of least square fit by taking globally occurred earthquake data. Accordingly, the m_b and M_S data set taken from ISC has been used in the present study.

To convert m_b, M_S, M_L and M_D in to moment magnitude Mw different global empirical relations developed by different authors (Scordilis 2006; Akkar et al. 2010; Das and Sharma 2011; Karimiparidari et al. 2013; Kadirioglu and Kartal 2016) have been used and compared with the existing mb-Mw and Ms-Mw pairs of data compiled from Global Centroid Moment Tenser (GCMT) having 133 and 119 events for mb-Mw and Ms-Mw pairs respectively. The regression relations for the conversion of m_b, M_S, M_L and M_D into moment magnitude Mw for the present study are:

m_b conversion into M_w

The empirical relation for M_w-mb pairs according to Scordilis (2006);

$$MW = 0.85(\pm 0.04)\text{mb} + 1.03(\pm 0.23), 3.5 \le m_b \le 6.2, R^2 = 0.53, \sigma = 0.29, n = 39,784, \quad (1)$$

The empirical relation for M_w -mb pairs according to Akkar et al. (2010);

$$MW = 1.104(\pm 0.03)mb - 0.194(\pm 0.16), 3.5 \le mb \le 6.3, \quad (2)$$

The empirical relation for M_w -mb pairs according to Karimiparidari et al. (2013),

$$M_w = 1.572622(\pm 0.022)\text{mb} - 3.071216 (\pm 0.092), 3.1 \le mb \le 6.0, \text{RMSE} = 0.47 \quad (3)$$

The empirical relation for M_w -mb pairs according to Das and Sharma (2011);

$$M_w = \frac{\text{mb} - (1.65 \pm 0.2)}{0.65 \pm 0.003}, 2.9 \le mb\ ISC \le 6.5, R^2 = 0.54, \sigma = 0.27, n = 23,245 \quad (4)$$

The Moment magnitude M_w is not directly available in GCMT data bank but the seismic moment (Mo) is observed in GCMT. Then, MW is computed from Mo for the corresponding (mb-Mw pairs) using Eq. (5);

$$M_w = \frac{3}{2}M_0 - 10.7, n = 133 \quad (5)$$

$$M_w = 0.6880m\text{b} + 1.86, 3.1 \le mb \le 6.5, R^2 = 0.99, n = 133\ (\text{OLS}) \quad (6)$$

$$M_w = 0.834m\text{b} + 1.181, 3.1 \le mb \le 6.5, R^2 = 0.99, n = 133(OR) \quad (7)$$

M_S conversion into M_w

The empirical relation for M_w-Ms pairs according to Scordilis (2006)

$$M_w = 0.67(\pm 0.04)\text{Ms} + 2.07(\pm 0.03), 3.0 \le M_s \le 6.1, R^2 = 0.77, \sigma = 0.17, n = 39,784 \quad (8)$$

The empirical relation for M_w-Ms pairs according to Akkar et al. (2010)

$$M_w = 0.571(\pm 0.02)\text{Ms} + 2.484(\pm 0.11), 3.0 \le Ms\ 5.5, \quad (9)$$

$$Mw = 0.817(\pm 0.03)Ms + 1.176(\pm 0.18), 5.5 \le Ms \le 7.5, \quad (10)$$

The empirical relation for M_w-Ms pairs according to Karimiparidari et al. (2013),

$$M_w = 0.623642(\pm 0.015)\text{Ms} + 2.289902(\pm 0.076), 3.0 \le Ms \le 6.1, \text{RMSE} = 0.19 \quad (11)$$

The empirical relation for M_w-Ms pairs according to Das and Sharma (2011)

$$M_w = 0.67(\pm 0.00005)\mathrm{Ms} + 2.12(\pm 0.0001),\quad 3.0 \le Ms \le 6.1, R^2 = 0.83, \sigma = 0.12,\ n = 24,807 \tag{12}$$

$$M_w = 1.06(\pm 0.0002)\mathrm{Ms} + 0.38(\pm 0.006),\quad 6.1 \le Ms \le 7.4, R^2 = 0.89, \sigma = 0.16, n = 2,250 \tag{13}$$

The empirical relation for M_w-Ms pairs according to Kadirioglu and Kartal (2016)

$$M_w = 0.59(\pm 0.03)\mathrm{Ms} + 2.46(\pm 0.12),\quad 3.0 \le Ms \le 6.1, R^2 = 0.80, RMSE = 0.18,\ n = 405 \tag{14}$$

$$Mw = 0.92\ (\pm 0.14) \times Ms + 0.51\ (\pm 0.9),\quad 6.1 \le Ms \le 7.4, R^2 = 0.86, RMSE = 0.15, n = 32 \tag{15}$$

From observed M_S for respective Mw, the regression relations were developed and are presented by Eqs. 16 and 17.

$$M_w = 0.506Ms + 2.943, 3.1 \le Ms \le 6.5,\quad R^2 = 0.99, n = 119(\mathrm{OR}). \tag{16}$$

$$M_w = 0.351Ms + 3.666, 3.1 \le Ms \le 6.5,\quad R^2 = 0.99, n = 119(\mathrm{OLS}). \tag{17}$$

M_L conversion into M_w

Since observed M_L data is not available for the corresponding Mw from GCMT catalog for the country, it is not possible to make any comparison with previous works for the validity of conversion from M_L to Mw. Accordingly, Karimiparidari et al. (2013) relation was used for conversion from M_L to Mw. The procedure used for the conversion by Karimiparidari et al. (2013) is first to see the relation between M_N (Nutili Magnitude) and M_L. Therefore, he has developed a relationship between M_N (Nutili Magnitude) and M_L with Eq. (18).

$$M_N = 0.90\ (\pm 0.03) \times M_L + 0.51\ (\pm 0.13), 2.7 \le ML \le 6,\quad R^2 = 0.78, RMSE = 0.15, n = 856 \tag{18}$$

This equation is valid within the magnitude range of $2.7 \le M_L \le 6$. The relationship is reliable with the RMSE = 0.23 and $R^2 = 0.78$ and this resulted in selecting the equation than the rest for the conversion. Hence, in order to convert M_L to M_W when only the M_L magnitude is known, as in the present case, first M_L is converted into M_N by using Eq. (18) and later M_N is converted into M_W by using Eq. (19) (Karimiparidari et al. 2013)

$$M_W = 0.67\ (\pm 0.09) \times M_N + 1.73\ (\pm 0.43),\quad 3.5 \le M_N \le 6.3, R^2 = 0.79, RMSE = 0.2, n = 67 \tag{19}$$

Finally, by using Eq. (19), the M_L magnitude events were converted into Mw for the catalog developed during the present study.

M_D conversion into M_w

Like M_L conversion into Mw as discussed above, the observed M_D was also not available for the corresponding Mw from GCMT catalog for the country. Therefore, it was not possible to make any comparison for the validity of conversion from M_D to Mw. However, it was attempted to review literatures to be used as conversion relations. Akkar et al. (2010) conversion equation (20) is relatively good R^2 and *RMSE*, hence this relation was used for conversion of M_D into M_W.

$$M_W = 0.764\ (\pm 0.04) \times M_D + 1.379\ (\pm 0.2),\quad 3.7 \le M_D \le 6.0, R^2 = 0.7, RMSE = 0.2, n = 673.2 \tag{20}$$

Mapping b-values

Once the catalogue is homogenized and completed in time and magnitude in Moment magnitude M_w scale at hand, b-values are calculated and mapped for selected regions using Zmap developed by Wiemer (2001). There are different ways to calculate b-values, most commonly, the maximum likelihood method by Aki (1965) is used for calculating b-value Therefore, in the present study, the maximum likelihood method is used with Bootstrapping which has shown to be a robust and unbiased estimation in most of the cases (Wiemer and Wyss 1997) for computation of b-values for respective regions. For an earthquake catalogue with mean magnitude M_{mean} and cutoff magnitude MC or the minimum magnitude (M_{min}) of the given sample the maximum likelihood gives;

$$b = \log_{10}(e) \Big/ (M_{mean} - M_C) \tag{21}$$

Shi and Bolt (1982) provided an improved formula to calculate the standard error of the magnitude-frequency b value by equation (22)

$$\delta b = 2.30b^2 \sqrt{\frac{\sum_i (M_i - \langle M \rangle)^2}{n(n-1)}} \tag{22}$$

where 'n' is the sample size. 'δb' in these calculations tends to underestimate the true standard deviation of 'b' because it assumes a correctly determined magnitude of completeness MC and a complete catalogue.

The number of earthquakes increases with decreasing magnitude. This size distribution of earthquakes in a seismogenic zone can often be described by a power law relationship. The earthquake frequency-magnitude distribution (FMD) describes the relationship between the frequency of occurrence and the magnitude of earthquakes (Ishimoto and Iida, 1939; Scordilis 2006).

The power law equation is given as equation (23)

$$\log N = a - bM \tag{23}$$

where N: the cumulative number of earthquakes with magnitude greater or equal than M. a and b are parameters that describe the FMD. The parameter **a** describes the productivity of the volume, and **b**, the slope of the frequency-magnitude distribution (FMD), describes the relative size distribution of events. This relationship is only valid down to the magnitude of completeness, Mc. Mc denotes the lowest magnitude at which 100% of the events in a space-time-volume are detected (Woessner and Wiemer 2005; Nasir et al. 2010; Alamilla et al. 2014).

For *b*-value and b-value mapping in the present study, a homogenized catalog into moment magnitude scale Mw with high quality data set during the period 1960–2016 were used (Fig. 2). The distribution of b-values and its spatial changes was mapped by using a grid of $0.2^0 \times 0.2^0$ for time period of 2003–2014 with Mc = 4.6 for Afar region including Red sea and Gulf of Aden rifts. Further, the b-value was computed for both Afar and Dabbahu volcano separately by using the grid size of $0.05^0 \times 0.05^0$ for a complete time period of 2005–2016 with Mc value of 4.8. Besides, the b-value map for NMER is computed with grid size of $0.1^0 \times 0.1^0$ for a time period of 2001–2003 with Mc value of 3.2. Similarly, the b-value for CMER is mapped by using a grid of size $0.1^0 \times 0.1^0$for a time period of 2001–203 with Mc value of 3.1. Finally, the b-value map for SMER was computed with a grid size of $0.1^0 \times 0.1^0$ for a time period of 1960–2016 with Mc value of 5.1. The four regions that were considered and discussed above are shown in Fig. 2 (SMER, CMER, NMER and Afar Rifts and Dabbahu MS(including Red sea and Gulf of Aden Rifts)).

Magnitude of completeness mc

Accurate knowledge of Mc is essential for mapping out a variety of different seismicity parameters such as 'a' -and b-values, it is recommended to estimate Mc as precisely as possible in order to maximize the number of events in the catalogue while at the same time not assuming a too low value for the magnitude of completeness so as not to lower the b-value too much.

Woessner and Wiemer (2005, 2005) have compared different methods on how to obtain the best possible value for MC. The details of the different methods such as EMR-Method (Entire Magnitude Range), Maximum curvature (MAXC), Goodness of-fittest (GFT), etc. are described in great detail by Woessner and Wiemer, 2005, b). In the present study, the MAXC method was used to evaluate Mc for different regions with their respective complete catalog in time and magnitude throughout the study.

Results and discussions

Results

Homogenized earthquake catalog of Ethiopia and its environs (1960–2016)

The empirical magnitude conversion equations for mb vs Mw presented in this study (see equations (6, 7)) are compared with the previously developed magnitude conversion equations (1, 2, 3, 4) respectively by different authors (Scordilis, 2006; Akkar et al., 2010; Das and Sharma, 2011; Karimiparidari et al., 2013).

The comparisons are given in Fig. 3(a) for mb into Mw conversions.

Similarly, the empirical magnitude conversion equations for Ms. vs Mw presented in this study (see equations (16, 17)) are compared with the previously developed magnitude conversion equations (8, 9, 10, 11, 12, 14, 15) respectively by different authors (Scordilis, 2006; Akkar et al., 2010; Das and Sharma, 2011; Karimiparidari et al., 2013; Kadirioglu and Kartal (2016). The comparisons are given in Fig. 3(b) for Ms. into Mw conversions.

The residual graphs are presented in Fig. 4(a) Residual graphs for Mw (obs) - Mw (est) Scordilis (2006) to mb, (b) residual graphs for Mw (obs)-Mw (est) to mb by Ordinary Least square (OLS) from this study, (c) mb vs Mw (observed), (d) Mw (obs)-Mw (est) to mb by OR from this study and Fig. 5(a), Ms. vs Mw (observed) (b) residual graphs for Mw (obs)-Mw (est) to Ms. by OR from this study, (c) Mw (obs)-Mw (est) to Ms. by OLS from this study, and (d) Residual graphs for Mw (obs) - Mw (est) Scordilis, 2006 to Ms.

It should be noted that the M_L and M_D estimates generally depend on the information disseminated by local seismic agencies. In addition, observed M_L and M_D were not available for the corresponding Mw from GCMT/HRVD catalogue for the country, therefore it was not possible to make any comparison for the validity of conversion from M_L and M_D to Mw. However, relations proposed by Karimiparidari et al. (2013) was used to develop conversion from M_L to Mw by using equation (18, 19). Relation proposed by Akkar et al. (2010) on the

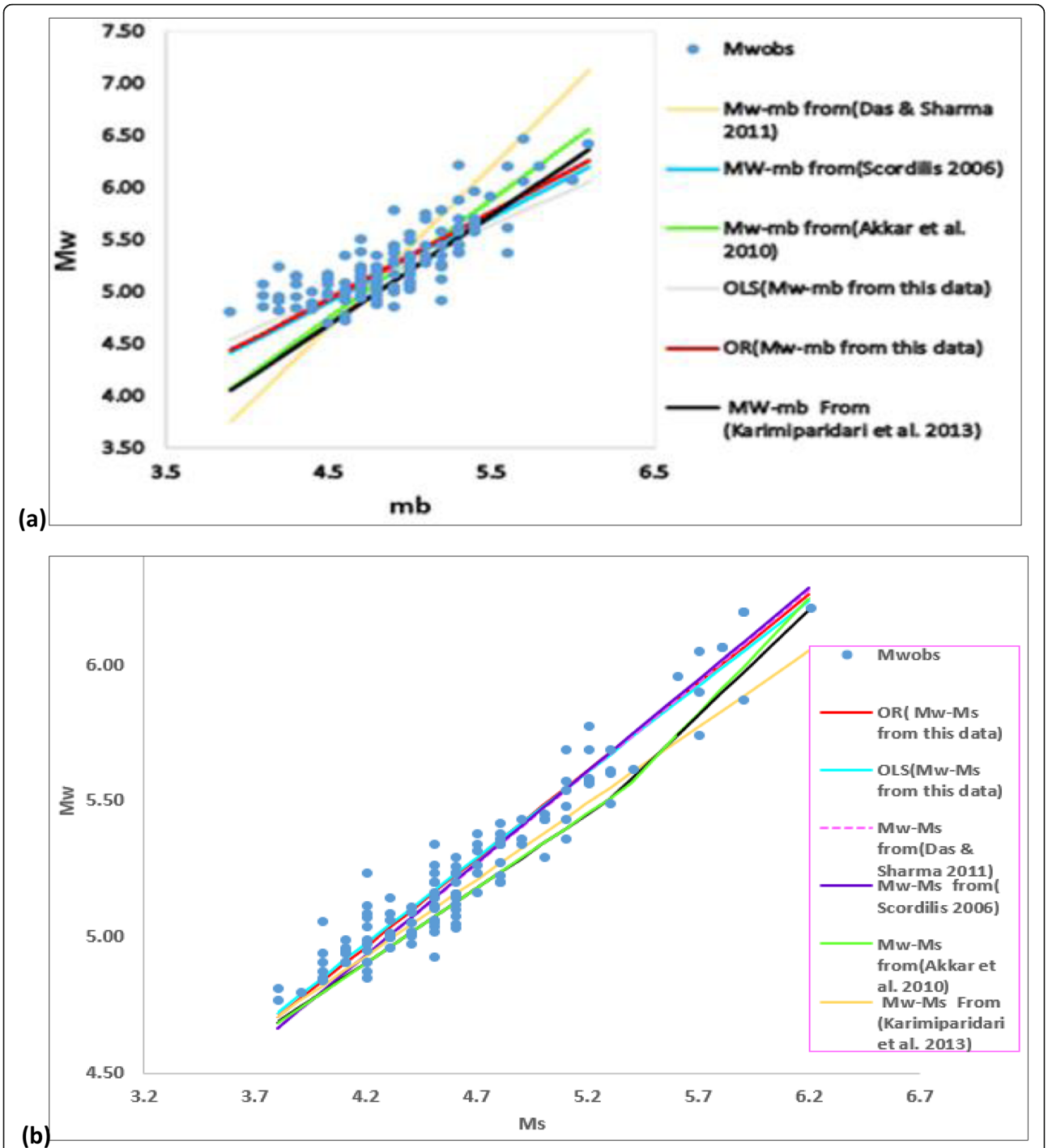

Fig. 3 (**a**) Result comparison MW versus m_b of this study and obtained by (Scordilis, 2006; Akkar et al., 2010; Das and Sharma, 2011; Karimiparidari et al., 2013) (**b**) Result comparison MW versus M_S of this study and obtained by (Scordilis, 2006; Akkar et al., 2010; Das and Sharma, 2011; Karimiparidari et al., 2013; Kadirioglu and Kartal, 2016)

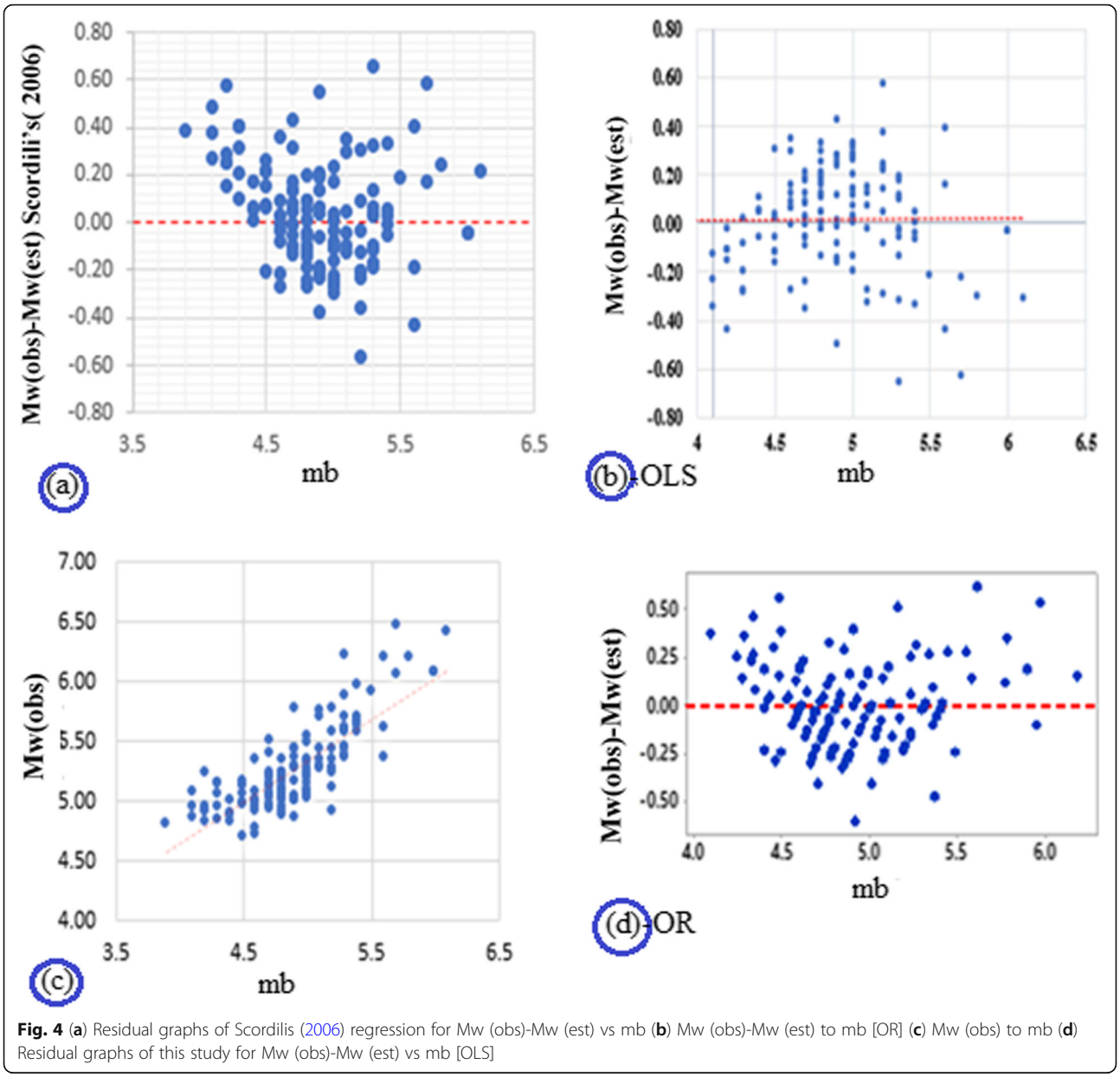

Fig. 4 (**a**) Residual graphs of Scordilis (2006) regression for Mw (obs)-Mw (est) vs mb (**b**) Mw (obs)-Mw (est) to mb [OR] (**c**) Mw (obs) to mb (**d**) Residual graphs of this study for Mw (obs)-Mw (est) vs mb [OLS]

other hand which has relatively good R^2 and *RMSE*, were used for the conversion of M_D to M_W by using equations (23, 24).

B-value maps of Ethiopian rifts including Red Sea and Gulf of Aden

Afar rift including Red Sea and Gulf of Aden In the present study, b-values were computed, and b-value maps were prepared for Ethiopian rifts (including Red sea and Afar Rifts). Further, Seismicity map of the regions were prepared using the homogenized catalogue in Moment magnitude scale and the new seismicity data for respective regions Figs. 2 and 6(a-f).

The seismicity parameters(Mc, a and b-values), the horizontal slices and the 3D b-value distribution maps for the Afar including Red Sea & Gulf of Aden Rifts have been determined The seismicity parameters such as the average a and b - values for this region respectively are a = 8.29 and b-value = 1.17 ± 0.05. The magnitude of Completeness (Mc) is equal to 4.6 ±0.03 and the period of completeness is from 2000 to 2014 (see Fig. 6(a-f)) and the Seismicity distribution / Commutative verses time following Gutenberg's law indicating that it is complete.

The middle portion of southern Red Sea at both depths 12 km and 28 km, are characterized by very high b-value of about 2.0 ± 0.05(see Fig. 7(a and b)) and the

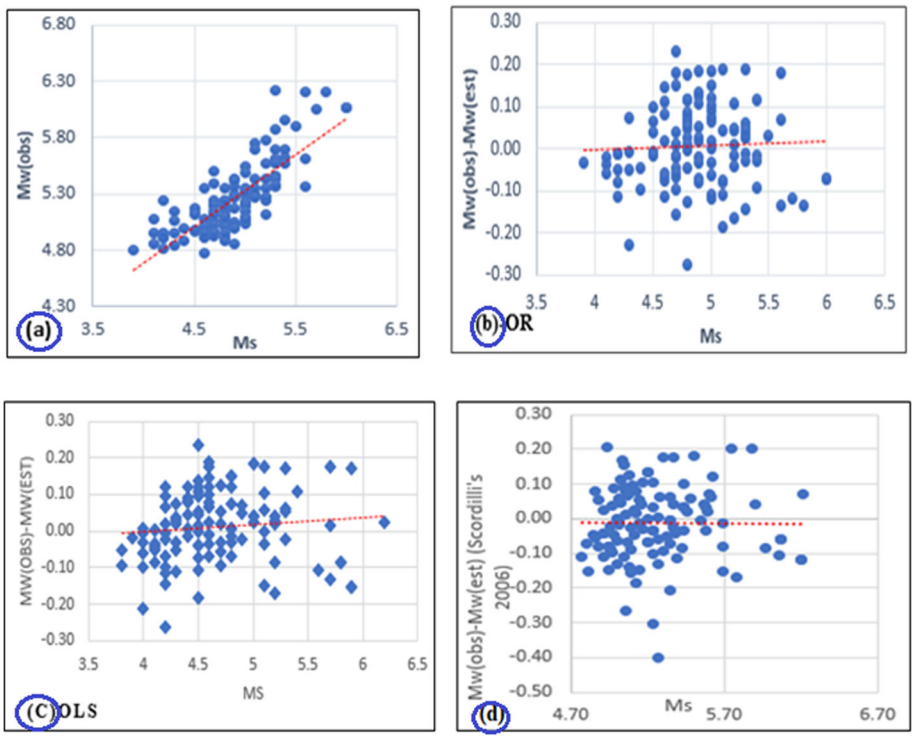

Fig. 5 (**a**) Mw (obs) to Ms. (**b**) Residual graphs of this study for Mw (obs)-Mw (est) vs Ms. [OR] (**c**) Mw (obs)-Mw (est) to Ms. [OLS] (**d**) Residual graphs of Scordilis (2006) regression for Mw (obs)-Mw (est) vs Ms.

3D b-value map (Fig. 7(c)) confirms that the high characteristics of b-value in the middle portion of southern Red Sea extends beyond the depth of 20 km. The North Red sea has relatively less b-value than that of the southern region and is about 1.2. This shows the Red Sea region is divided in to two seismic sources. From the b-value and Seismicity distribution points vie it is observed that the northern part of the southern red sea has different b-value features than the middle part of the Red sea as indicated in Fig. 7(a and b).

In Afar rift there are areas where b- values are high and low. The central Afar region has relatively normal b-value of about 1. However, in the south-west Afar region and the north-east of Afar region has high b-value of about 1.5. The Gulf of Aden Rift has b-value in the range of 1.1 to 1.2 which is the elevated b-value in the region.

Afar rift and Dabbahu volcano Afar rift and Dabbahu volcano were investigated by using 3D b-value map separately to see the relationship between the b-value and the tectonics of the magma induced seismicity in the rift. The spatial and temporal variations in the distribution of seismicity and stress accumulation are characterized by b-values for the Afar rift (Fig. 8(a)-(d)) and the Dabbahu volcano separately (Fig. 9(a-e).

From Fig. 8(d), under the Dabbahu, Hararo, Erta'ale, Asel volcanoes and other yet two unknown magmatic segments (MS) have high b-values (1.25–1.8). Immediately under the Dabbahu volcano, it is clearly seen that the b-value is very high and is about 1.8.

With the same seismicity parameters for the Afar rift but different grid size of 0.05^0*0.05^0, a separate 3D map of b-values is developed for Dabbahu volcano with respective 2D b-value slices as shown in Fig. 9(a-e).

NMER The Seismicity map, magnitude of completeness, average values of Seismicity parameter(a and b-values) and variations of b-value with time in years for the NMER are shown in Fig. 10(a-e).

The seismicity parameters such as average a and b-values for this region respectively are a = 4.0, b-value = 0.702 ± 0.07. The magnitude of Completeness (Mc) = 3.1 and period of completeness is from 2001 to 2003.This shows the Seismicity distribution /Commutative versus time follows Gutenberg's law showing that it is complete as shown in Fig. 10(a-e). The b-value depth slices of the NMER at depth of 0.1 km, 5 km, 7 km and 15 k are shown in Fig. 11(a-d) respectively. The 3D map of the b-value of the NMER is shown in Fig. 11(e).

CMER Seismicity map, Cumulative number of events vs time-straight-line trend, Magnitude of Completeness

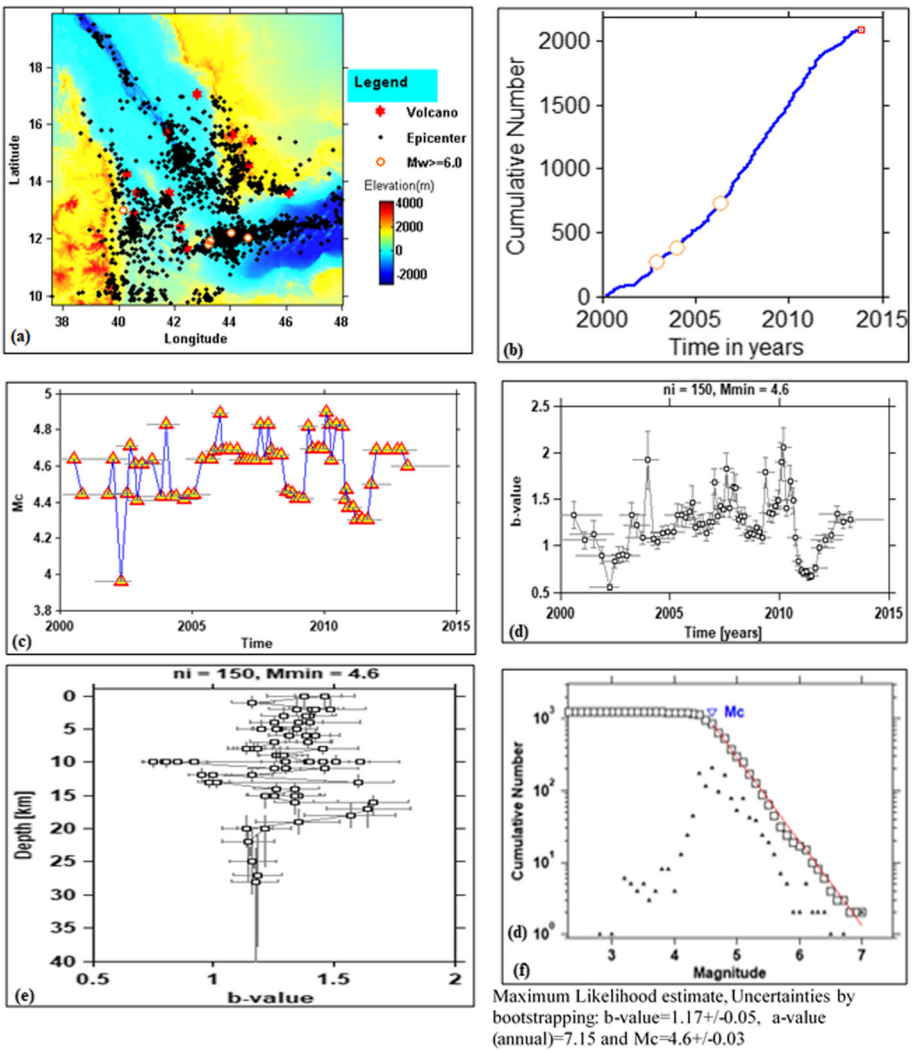

Fig. 6 Afar Rifts (Including Red Sea and Gulf of Aden): (**a**) Seismicity map of the region (**b**) Cumulative number of events vs time-straight-line trend -relatively complete (**c**) Magnitude of Completeness (Mc) with time (**d**) Temporal variation of b-value with period of completeness, ni = 150, Mmin = 4.6 (**e**) Spatial variation of b-value with depth, ni = 150, Mmin = 4 (**f**) average b and a-values of the region by maximum likelihood solution

with time, b-value variation over the magnitudes in Mw scale, ni = 80, Mmin = Mc = 3, average values of seismicity parameters(a, b values and Mc). Depth slices and 3D map of b-value for CMER at depth of 0.1 km, 7 km, 15 km and the 3D b-value map showing the features in 3D of the Central Main Ethiopian Rift (CMER) are shown in Fig. 12(a-i) respectively. The Central MER is bounded by the Yerer-Tullu-Wellel volcano-tectonic lineament to the north and the Goba–Bonga lineament to the south (see Fig. 13). It is also bounded to the east and west by fault escarpments.

The major magmatic segments in CMER are shown in Fig. 12(f-i). Some of these are Aluto MS, Aluto-Gedemsa MS and Boset-Kone MS and the Guraghe boarder fault (GBF).

The high b-value signatures were observed at 0.1 km depth beneath all the magmatic segments mentioned above and Guraghe BF, however there is no high b-value signature beneath Aluto-MS and is slightly seen at this depth Fig. 12(f). At 7 km depth Fig. 12(g) beneath all mentioned features above except the Guraghe BF indicates high b-value anomaly. The high b-value anomaly is started to diminish beneath Guraghe BF. At 15 km depth the major magmatic segments in Fig. 12 except the Guraghe BF. The Boset -Kone MS is increased in width and length and becomes continuous till this depth but it was

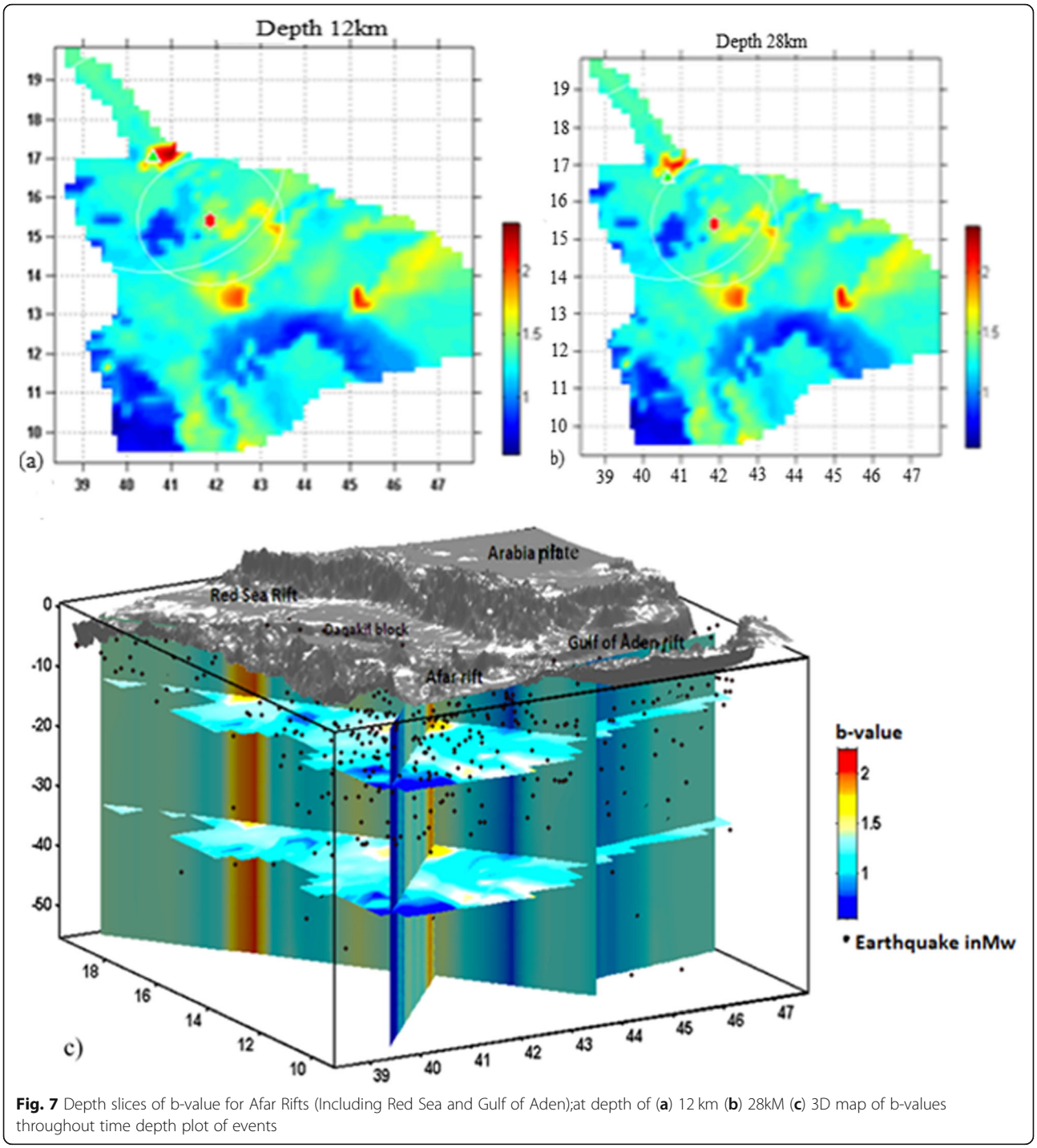

Fig. 7 Depth slices of b-value for Afar Rifts (Including Red Sea and Gulf of Aden);at depth of (**a**) 12 km (**b**) 28kM (**c**) 3D map of b-values throughout time depth plot of events

discontinuing between 0.1 and 7 km slice depth, the Guraghe BF is not observed well at this depth.

SMER The seismicity parameters for the SMER such as the average a and b- values for this region respectively are a = 6.9, b-value = 1.03 and the magnitude of Completeness (Mc) = 5.1 Fig. 14(c). The period of completeness is from 1960 to 2016 shows the Seismicity distribution /Commutative versus time follows Gutenberg's law showing that it is complete Fig. 14(b).

The high b-value signatures were observed throughout the depths between 0.1 km to 35 km dipping in South East- south west and north of SMER with high b-values. The central part of SMER has relatively normal(b-value = 1) and low b-value near the volcano represented in the map. At 0.1 km depth, the high b-value is very

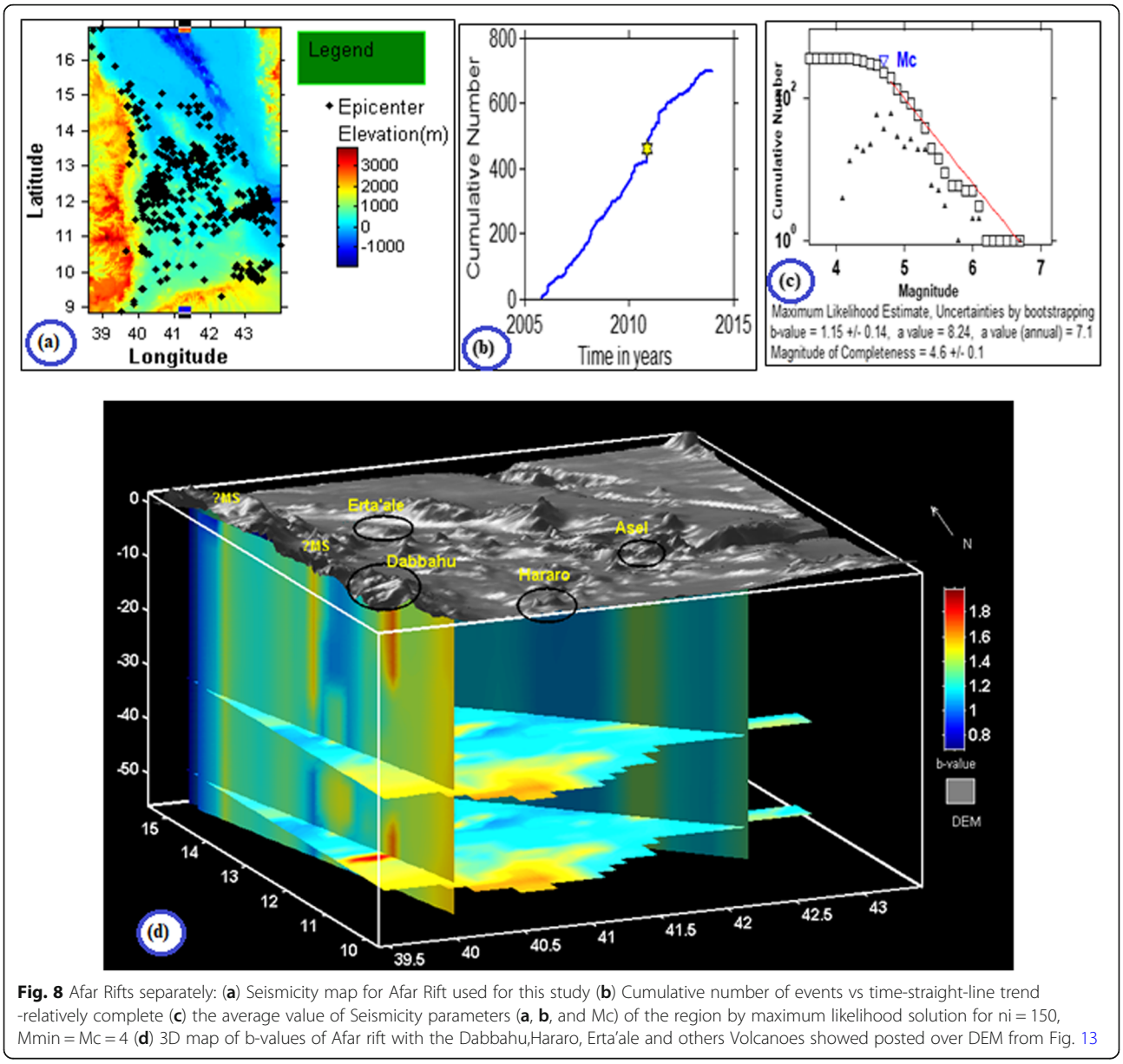

Fig. 8 Afar Rifts separately: (**a**) Seismicity map for Afar Rift used for this study (**b**) Cumulative number of events vs time-straight-line trend -relatively complete (**c**) the average value of Seismicity parameters (**a**, **b**, and Mc) of the region by maximum likelihood solution for ni = 150, Mmin = Mc = 4 (**d**) 3D map of b-values of Afar rift with the Dabbahu,Hararo, Erta'ale and others Volcanoes showed posted over DEM from Fig. 13

close and to the north of the volcano represented in the map.

Discussions

Homogenized catalog of Ethiopia and its environs

In both mb and Ms conversion into Mw relationships, estimates by Scordilis (2006) approach yielded results that are closer to the orthogonal regression (OR) relationships of the results of the present study (see Fig. 3(a-b)). This also confirmed by the residual graphs presented in Fig. 4(a) Residual graphs for Mw (obs) - Mw (est) Scordilis, 2006 to mb, (b) residual graphs for Mw (obs)-Mw (est) to mb by Ordinary Least square (OLS) from this study, (c) mb vs Mw (observed), (d) Mw (obs)-Mw (est) to mb by OR from this study and Fig. 5(a), Ms. vs Mw (observed) (b) residual graphs for Mw (obs)-Mw (est) to Ms. by OR from this study, (c) Mw (obs)-Mw (est) to Ms. by OLS from this study, and (d) Residual graphs for Mw (obs) - Mw (est) Scordilis, 2006 to Ms.

The scatters plots in Fig. 4(b and d) almost show closer results but Fig. 4(d) in random variations suggests unbiased estimations of Mw from mb magnitude scales than Fig. 4(b). The orthogonal regression (OR) relation developed for the observed data of mb-Mw pairs agrees well with the work of Scordilis (2006) regression.

In the same way the scatters plots in Fig. 5(b) show the same results with the Scordili's Fig. 5(d) than the

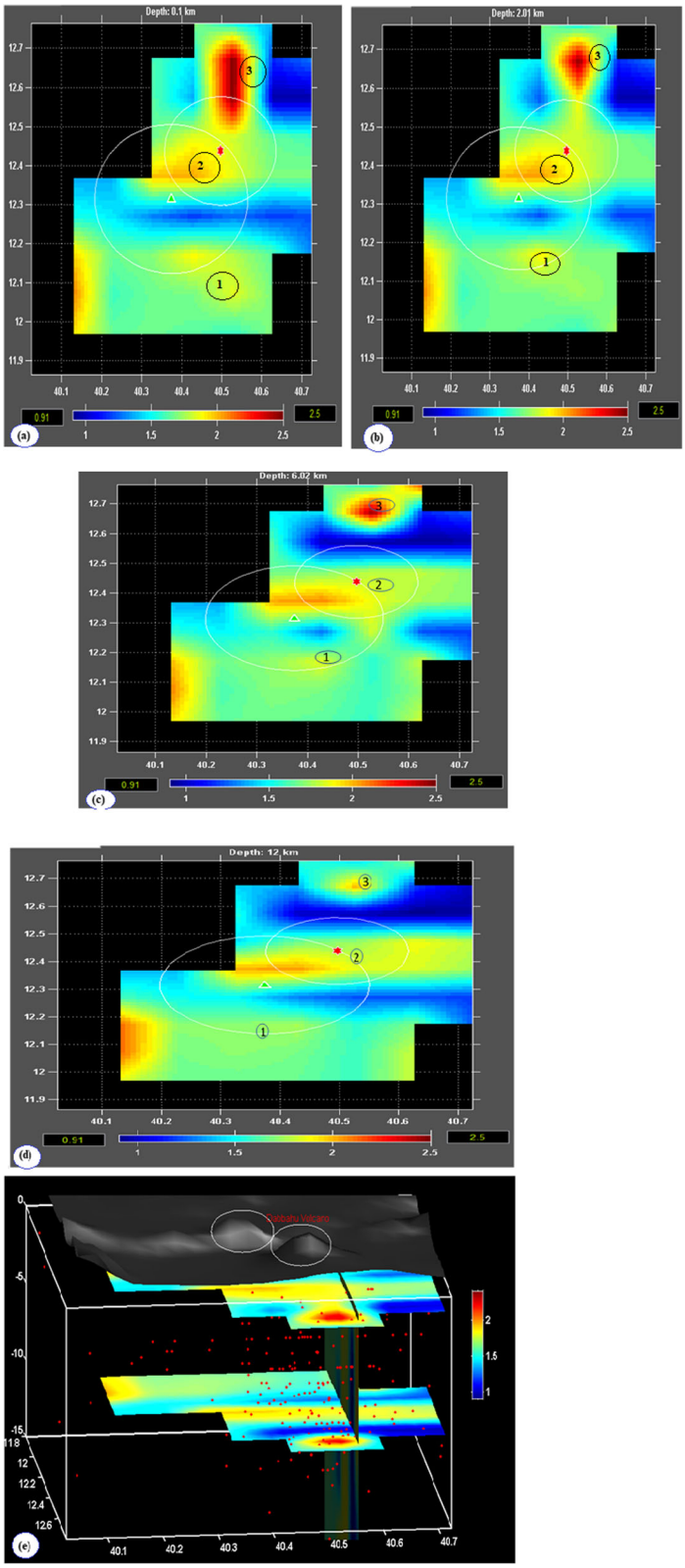

Fig. 9 Dabbahu Volcano: The depth Slices of b-value at depth of: (**a**) 0.1 km (**b**) 2 km (**c**) 6 km (**d**) 12 km (**e**) 3D b-value map of the Dabbahu Volcano, we can see the migration (depth and lateral variation) of the magma chambers beneath the Dabbahu Volcano showed in DEM on top indicated by the high b-values, the red symbol(•)showed in this map is the EQ events

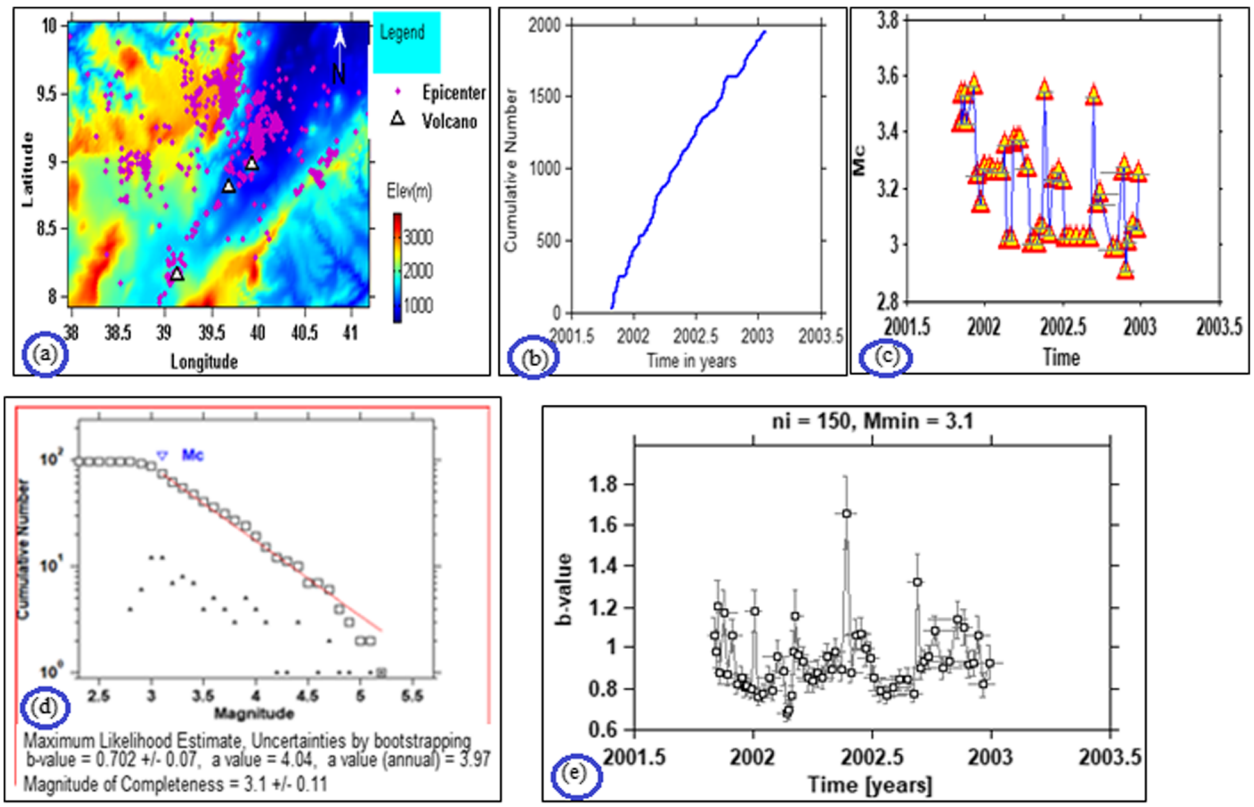

Fig. 10 Northern Main Ethiopian Rift (NMER): (**a**) Seismicity map of NMER (**b**) Cumulative number of events vs time-straight-line trend -relatively complete (**c**) Magnitude of Completeness (Mc) with time (**d**) the average value of Seismicity parameters (a, b, and Mc) of the region (**e**) Temporal variation of b-value with period of completeness, ni = 150, Mmin = 3

residual plot of Fig. 5(c) indicating the random variations suggests unbiased estimations of Mw from Ms. magnitude scales than Fig. 5(b).

In case of Ms. vs. Mw relationship, estimates by Scordilis (2006) yield closer results to this study of the orthogonal regression relationships. This is also confirmed by the residual graphs Fig. 4d and are close to zero residuals than residuals in OLS Fig. 4b. In the case of Ms-Mw pairs regressions Fig. 3(b) and residuals and Fig. 5(b) of the OR than OLS Fig. 5(c) is again in good agreement with Scordilis (2006). On the other hand, the relationship proposed by (Akkar et al., 2010; Das and Sharma, 2011; Karimiparidari et al., 2013; Kadirioglu and Kartal, 2016) for both MW-mb and Ms. pairs has calculated slightly lower MW estimations when compared to the present study results and the estimations by Scordilis (2006) relation.

It should be noted that the M_L and M_D estimates generally depend on the information disseminated by local seismic agencies. In addition, observed M_L and M_D were not available for the corresponding Mw from GCMT catalogue for the country, therefore it was not possible to make any comparison for the validity of conversion from M_L and M_D to Mw.

However, relations proposed by Karimiparidari et al. (2013) was used to develop conversion from M_L to Mw by using equation (18) and (19). Relation proposed by Akkar et al. (2010) on the other hand which has relatively good R^2 and *RMSE*, were used for the conversion of M_D to M_W by using equations (23) and (24). Therefore, using above regression relations, about 3814 earthquake events were left as a new Homogenized Earthquake catalogue of Ethiopia and its environs during the last 56 years (1960–2016) with a magnitude of ≥3Mw, showing a consistent pattern of cumulative rate changes. In the present study, it has also been confirmed that the Orthogonal regression relations are stronger relations than OLS for the earthquake magnitude conversions.

b-value characteristics of Ethiopian rifts including Red Sea and Gulf of Aden

Afar rift and Dabahu magmatic segment including Red Sea and Gulf of Aden

The Northern and Southern portions of the southern red sea do have unique character of larger earthquakes (in 1967, Mw = 6.1, 6.2 and Mw = 6.7 in same year and 1993, Mw = 6.7) that agrees well from the b-value characteristics of these regions. These two regions have unique b-values.

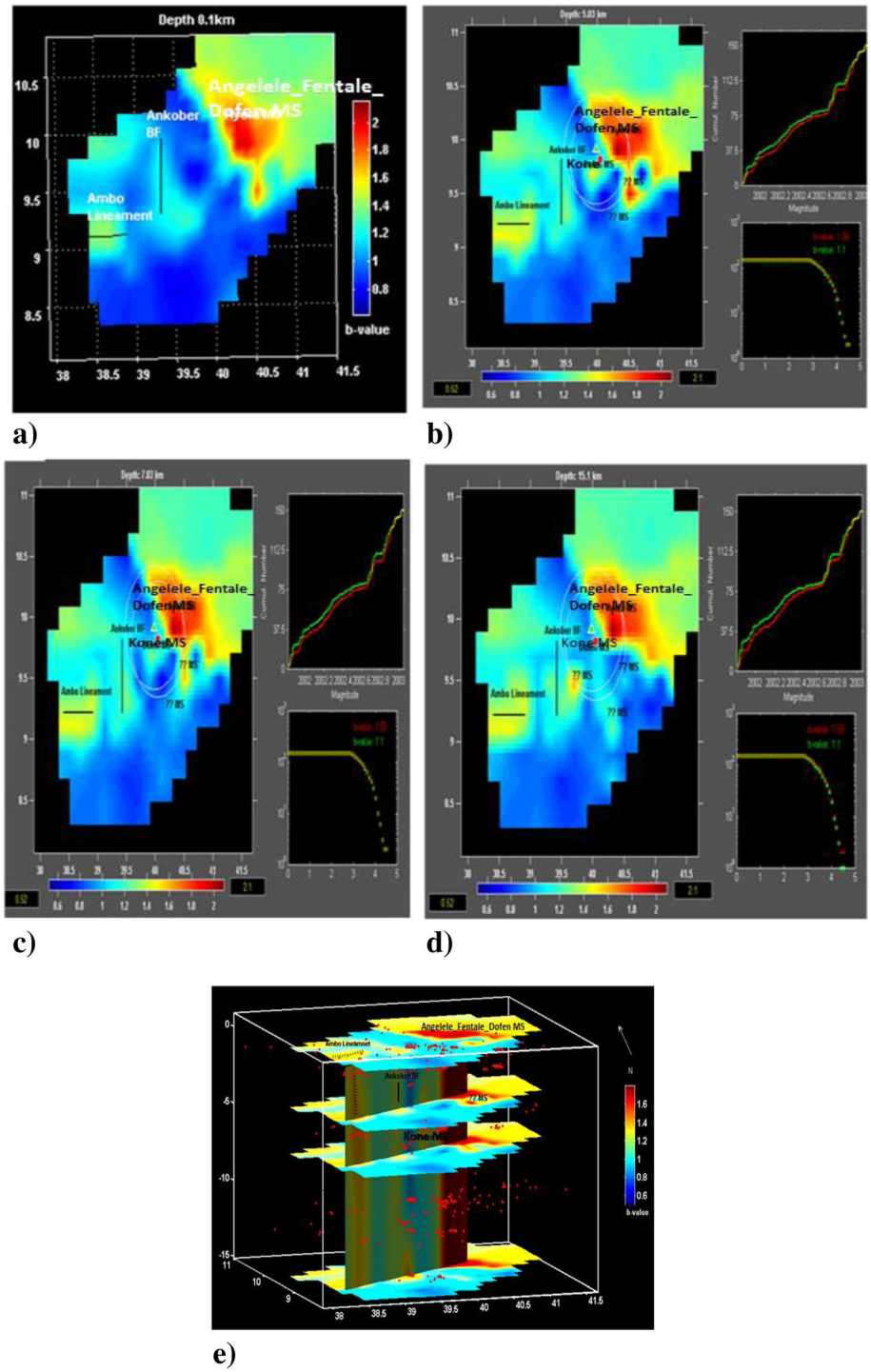

Fig. 11 Depth Slices of b-values for NMER at depth: (**a**) 0.1 km, (**b**) 5 km (**c**)7 km (**d**) 15 km (**e**) 3D map of b-value with red dot posted over it showing earthquake events in Moment magnitude Mw ≥ 3.0 within the specified period of completeness Fig. 10(b). The black horizontal and vertical lines are indicated respectively by Ambo lineament and Ankober boarder faults

The Northern Region of Southern red sea has lower b - value of about 1.1 and Southern portions has higher b-value equal to about 1.5.(see Fig. 7(a and b)). This implies large proportion of smaller number of magnitude of earthquakes are more concentrated in the Northern portion than in the southern portion of the red sea, that had only one large earthquake of magnitude of 6.1 in 1988 as shown in Fig. 2 during 1960–2016. Besides, Northern Red

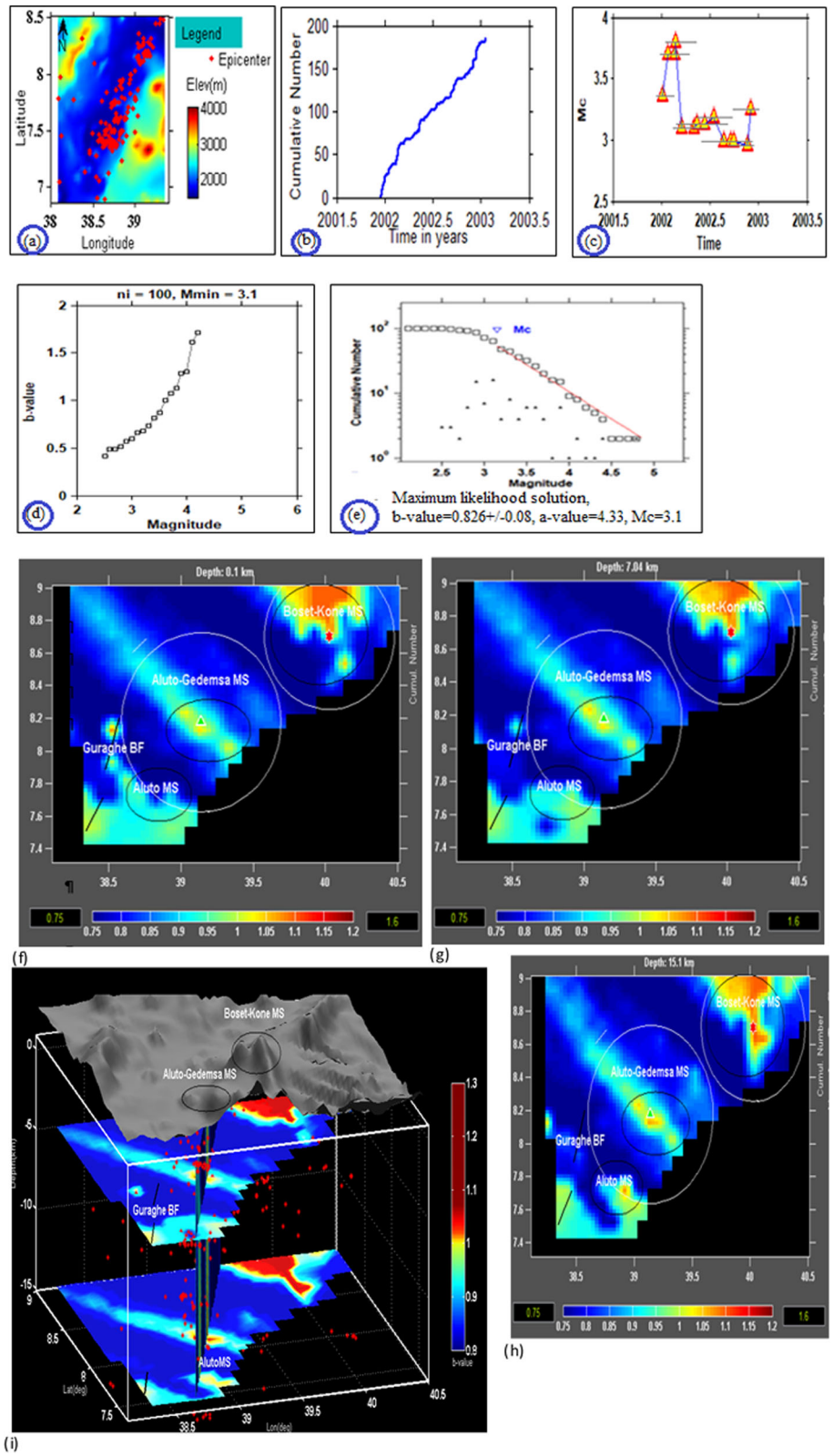

Fig. 12 (See legend on next page.)

(See figure on previous page.)
Fig. 12 Central Main Ethiopian Rift (CMER): (**a**) Seismicity map of CMER (**b**) Cumulative number of events vs time-straight-line trend -relatively complete (**c**) Magnitude of Completeness (Mc) with time (**d**) b-value variation over the magnitudes in Mw scale, ni = 80, Mmin = Mc = 3.1 (**e**) average values of seismicity parameters(a, b values and Mc)using maximum likelihood method. Depth slices and 3D map of b-value for CMER at depth of: (**f**) 0.1 km, (**g**) 7 km, (**h**) 15 km and (**i**) the 3D b-value map showing the fetures in 3D, the two horizontal slices at 5 km and 15 km depth and one vertical slices supperimossed by DEM showig Aluto-Gedemsa and Boset kone volcanoes circled by black color. The red dots show the Earthuake events ditribution along the depth indicted

Sea (north of 18°N) is characterized dominantly by normal faulting events (Hofstetter and Beyth, 2003) this also confirmed by relatively by high b-value and the southern region has mixed focal solutions including dominantly reverse mechanisms and strike - slip motions (Hofstetter and Beyth, 2003).

From Fig. 6(d), it can be seen that b-value decreases from time period 2010 to 2011 indicating that the seismic activity has been increasing in this time range and it also suggests that abrupt increase around 2011 Fig. 6(b) in the region. The Gulf of Aden Rift has b-value more than 1 in the range of (1.1 ±0.5)-(1.3 ±0.7) at both 12 km and 28 km depth) (see Fig. 7(a and b)) indicating that increased material heterogeneity or crack density has resulted into high b-values (Mogi, 1962) beneath the rifts.. This suggests an increase in applied shear stress (Scholz, 1968) or an increase in effective stress (Wyss, 1973) decreases the b-value. Many evidences suggest that b can act as a stress meter in the crust which came from the fact of asperity (Wiemer and Wyss, 1997; Prasad and Singh, 2015).

There is an abundance of seismic activity on land that is conformed by the high b-value anomaly, west of the Gulf of Aden, and in the Gulf of Aden, which is mainly in the ENE – WSW direction (see Fig. 7(a and b)). Further, Hofstetter and Beyth (2003) and Manighetti et al. (2001) have indicated a mixture of normal faulting and left - lateral strike - slip movements along NW–SE - striking fault planes. The WSW–ENE is spreading centre of the Gulf of Aden that propagates westward up to the Danakil - Aysha'a block. Aysha'a. Fault plane solutions of some events suggest normal faults with a fault plane striking E–W to ENE–WSW. According to Vergne et al.

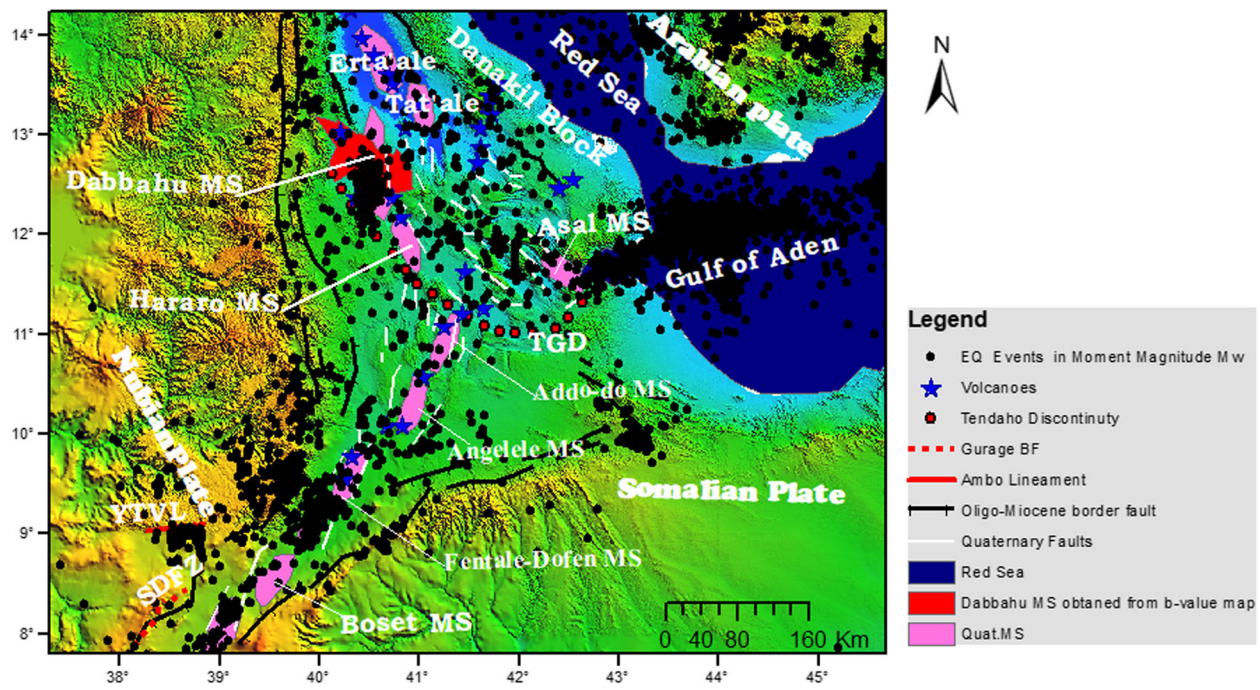

Fig. 13 Location of the Dabbahu rift segment within the Afar triple junction zone; major fault zones. Danakil Block is a microplate between the Nubian and Arabian plates. Red shading indicates 50 km-long magmatic segments (MS)—zones of dense faulting and aligned Quaternary eruptive centers—the current locus of strain within Afar (after C J Ebinger et al., 2008, b and reference therin). The black dots show the earthquake events in moment magnitude scale Mw from this study superimposed on a digital elevation model (Shuttle Radar Topography Mission data-30 m resolution). Inset: the location of SDFZ: Silti-Debre Zeit Fault Zone, YTVL: Yerer Tulu-Volcano Lineament, Red solid line: Ambo Lineament, Red doted line: Guraghe BF-Gurage border Fault, the curved formed by red dotes is TGD:Tendaho-Goba'aDiscontinuity, The blue star shows the Volcanoes in the rift, and the red polygon shows high b-value from Fig. 9 representing the Dabbahu Magmatic segment

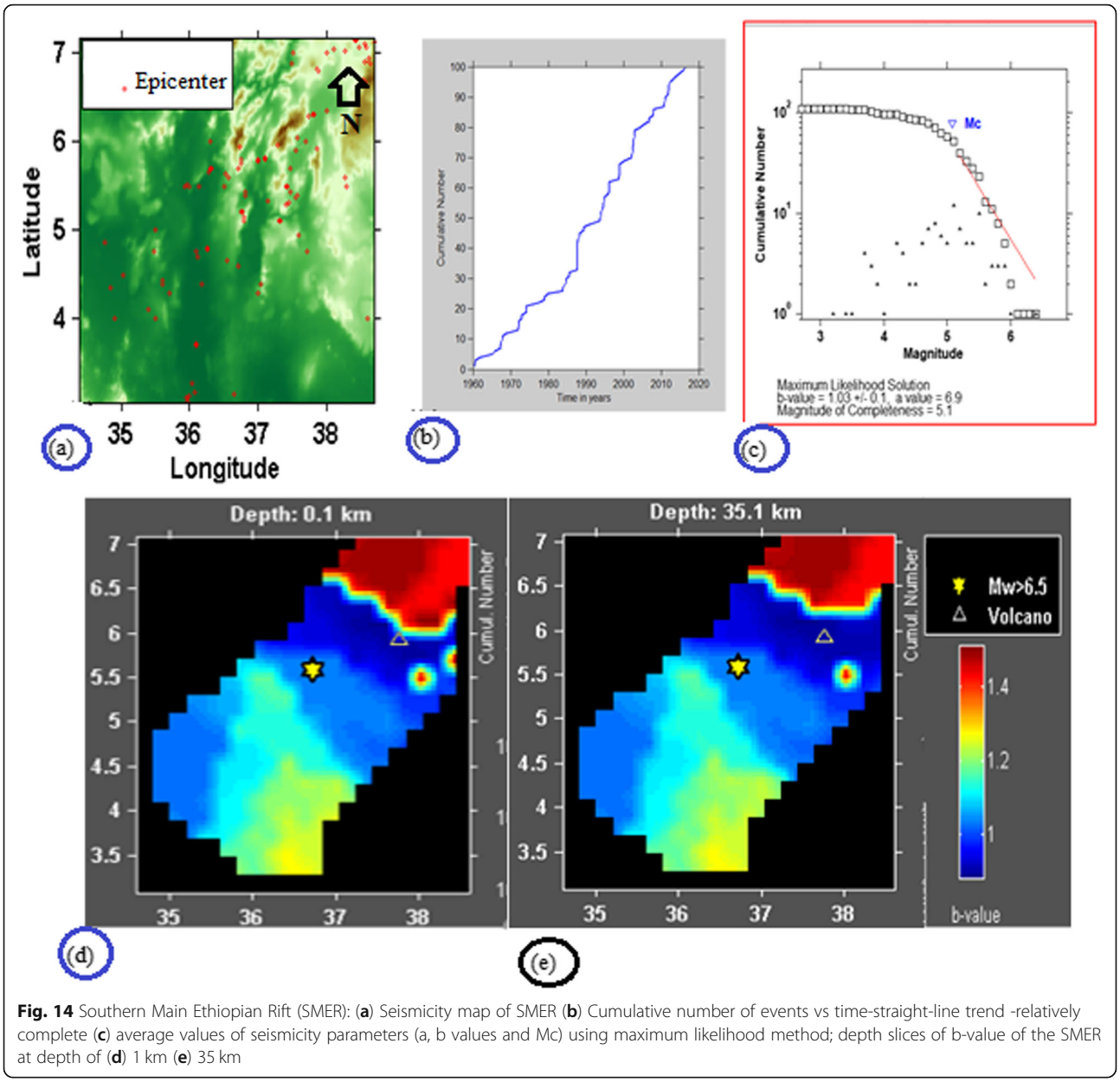

Fig. 14 Southern Main Ethiopian Rift (SMER): (**a**) Seismicity map of SMER (**b**) Cumulative number of events vs time-straight-line trend -relatively complete (**c**) average values of seismicity parameters (a, b values and Mc) using maximum likelihood method; depth slices of b-value of the SMER at depth of (**d**) 1 km (**e**) 35 km

(2016), the Gulf of Aden rifted margins transition from being volcanic being magmatism in the west to non-volcanic or including little evidence of magmatism in the east (Ahmed et al., 2014) this confirms that high b -value on the western side than on the eastern side of Gulf of Aden (see Fig. 7(a and b)). Besides, most of the active zones of the Afar Depression including the Dobi cluster and Serdo sequence as shown in Figs. 1 and 13, respectively are found around 42°E and 12°N and to the west around 41.8°E and 12°N. From focal mechanisms, the Dobi is almost all Normal faults and the Serdo is strike-slip motion where b-values are high and low respectively in these regions. The distinguished tectonic features of this region are the Tendaho Goba'ad discontinuity (TGD) and various known and unknown magmatic segments to produce magma induced seismicity in the region (See Fig. 13 and Fig. 9).

In the review article by Wiemer and Wyss (2002) cited in (Murru et al., 2007), elevated b-values (low stress areas) in the proximity of a volcano can be used to model the location, the size and the morphology of a magma chamber or the funnel of the volcano (Rierola, 2005). The b-value mapping is also a useful tool to display variation of stress accumulation over large areas. Generally, it is agreed that large earthquakes occur in high stressed areas (low b) and no large earthquake took place in high b areas (Nuannin, 2006) but swarms of earthquake like that of NMER (See Fig. 13 and 10).

A lower value of b implies that the region is under higher applied shear stress, and a higher value of b indicates that the area is already gone through the tectonic events. Spatial variations of b-value have also been studied by several researchers in number of seismically active areas (Wiemer and Benoit, 1996; Farrell et al., 2009; Singh et al., 2015). Observations of b-values in space reflect locally the effective stress (Scholz, 1968). From the Fig. 8(d), it can be seen that under the Dabbahu, Hararo, Erta'ale, Asel volcanoes and other yet two unknown magmatic segments have high b-values (1.25–1.8) showing the dyke injection, surface fissuring and volcanic eruption in Afar with associated swarm of earthquakes acmes the potential seismic hazard of rift zones in Ethiopia (Keir, 2006). As cited in Ebinger et al. (2008, b), the Red Sea, Gulf of Aden and East African rift arms formed within a Palaeogene flood basalt province associated with the Afar mantle plume (Yirgu et al., 2006). The thermal anomaly associated with the Palaeogene mantle plume persists today, as shown by low P- and S-wave upper-mantle velocities beneath the uplifted plateaux of Arabia and NE-Africa (Debayle et al., 2001 and Benoit et al., 2003) Bastow et al. 2005; Benoit et al. 2006). Hence, the spatial 3D b-value map prepared during present study for these three regions showed variation of the volcansim with depth and laterial variation of the low velocity zones respectivelly, which are confirmed by the high and the low b-values associated with occurance of Large earthquakes (eg.1915.7,Mw = 6.8 occurred in the south-west red sea riftas shown in Fig. 7(a, b and c), respectively. The three rifts have high b-values in their repective magma chambers and low b-values where large earthquake phenomenon were observed.

The study also showed the movement of the magma chambers with the depth as it can be seen from Fig. 9(a-e), it can be clearly seen that there are three markedly observed high b-value Anomalies beneath the Dabbahu volcano having different thicknesses and lateral extensions in all depths.

Three high b-value anomalies indication of magma chambers were observed at 12 km, 6 km, 2 km and 0.1 km depths.

At 12 km depth Fig. 9(d):

The (1st), (2nd) and (3rd) magma chambers are distinctly observed with high b-value respectively in between longitude (40.15° - 40.6°) and latitude (12 ° - 12.2 °), longitude (40.35 ° - 40.7 °) and latitude (12.35 ° – 12.5 °) and longitude (40.45 ° - 40.6 °) and latitude (12.65 ° - 12.75 °). Further, at this depth, the three magma chambers are separately observed.

At 6 km depth Fig. 9(c):

The 1stand 2nd high b-value anomalies-magma chambers started to be connected with different lateral extension than they were at 12 km depth but the 3rd magma chamber is observed with different lateral extension than what it was at 12 km depth.

At 2 km depth Fig. 9(b):

The 2nd magma chamber is diffused and connected to 3rd and detached from the 1st with different lateral extension than what it was at 12 and 2 km depth.

At 0.1 km depth Fig. 9(a):

The 3rd and 2nd magma chambers are fully connected with the 3rd and increased its length in latitude and it thinned in longitude directions.

Therefore, as can be seen from Fig. 9(a-d), there are spatial high b-value anomalies migration which probably linked to migration of magma chamber beneath Dabbahu volcano.

Generally, it is agreed that large earthquakes occurs in high stress areas (low b) and no large earthquake took place in high b value areas (Nuannin, 2006) however swarms of Earthquake and present study results also conforms this fact Fig. 7(a-c). The high b value anomalies (low Stress) are regions of increased crack density, and/or high pore pressure, related to the presence of nearby magma storage and this interpretation is supported by all the available geophysical evidence, such as tomographic studies and geodetic deformation measurements in the study regions (Ebinger et al., 2008, b). The magma induced seismicity for Africa is discussed and confirmed by different author (Aki, 1984; Wiemer and Benoit, 1996; Rierola, 2005; Keir, 2006; Ebinger et al., 2008, b; Feng et al., 2009; Trebbin and Wassermann, 2010; Prasad and Singh, 2015).

The dyke -induced Seismicity in the MER and the Dabbahu Seismicity by the Magma injection has been discussed by (Keir, 2006; Ayele et al., 2007, 2015; Ebinger et al., 2008, b). The Dabbahu rift event occurred in the southernmost Red Sea rift north of the Afar triple junction as indicated in Fig. 13 (Ebinger et al., 2008, b). This fact is evident by high b-value signature. The emplacement of magma and the accompanying crustal extension, as suggested by Keir (2006) and Ebinger et al. (2008, b) for the high crustal deformation rates would give rise to factors responsible for high b-value measurements in this regions (see Fig. 9(a-e)). These may be associated with mainly high heterogeneity of the crust due to numerous cracks from the increased stress and a high thermal gradient, which is also supported by focal depth distribution. The period of uplift and the period of high b-values overlap in time, these could be the underlying reasons for the high b-values measured in the present study area. The area of high b-values of 1.8 ± 0.05 in Dabbahu Magmatic segment may also be a result of magmatic fluids migrating from the Dabbahu volcano (see Fig. 9(a-e)).

In general, the presence of magma gives rise to the main factors causing higher b-values, mainly high heterogeneity,

and high thermal gradient. The presence of partial melt causes higher temperatures. In turn, a zone of relatively lower stress around the area of partial melt is created in the Dabbahu volcano-magmatic segment which is represented by high b-value signature (Fig. 9(a-e)).There is slight difference between the position and direction of the Dabbahu MS with the present study and pervious study. In the present study it is placed in North-west. However in the previous study it was almost placed in north (Ebinger et al., 2008, b) (see Fig. 13). The high temperatures in the lower crust made this layer ductile that has possibly reduced the strength of the material and thus, would not allow significant stress buildup (less stressed rift) within it (Ebinger et al., 2008, b).

The Main Ethiopian rifts (MER)

The magma induced seismicity in the NMER is highlighted in this study by b-value maps for some known magmatic segments as shown in Fig. 11(a-e) and Fig. 13. The high b-values (the low stress region) is associated with the swarms and it represents regions where already stress is released because of the magma eruption and migration, the eruption centers shown in Fig. 13 (after Keir, 2006; Ebinger et al., 2008, b) with high temperature, material heterogeneity and magma chamber migration. As a result, the magma induced swarms of earthquake has happened in the area, as shown in Fig. 10(a). Generally, in the NMER the average b-value is low (0.702 ∓0.07). The low b-values indicate high stress region with large magnitude earthquakes occurrence in this rift. Further, Natural Hazards associated with seismicity and volcanic eruptions poses a serious risk to life and economy in the NMER. In this rift there are also places that are characterized by high and low signature of b-values, indicating less and high stressed features, respectively.

From the Fig. 11(a) at depth of 0.1 km, it is clearly observed that the high b-values exist beneath the Ambo Lineament, Ankober boarder Fault (about b-value = 1.2–1.5). Also, very high b-value exist at North east of Ankober Fault segment. This is Angelele_Fentale_ Dofen Magmatic Segment (MS) (abot b-value = 1.6–2) which include Kone Ms. located in South of Angelele_Fentale_ Dofen_MS. The b-value depth slices of the NMER at depth of 0.1 km, 5 km, 7 km and 15 k are shown in Fig. 11(a-d).

At 5 km depth (Fig. 11(b)), all the high b-values that were observed at a depth of 0.1 km are also observed here and another high b-value anomaly is observed south-west of Angelele_Fentale_Dofen_MS which is around Kone_MS where it has not been observed at depth of 0.1 km. In addition, at this depth the high b-value anomaly is present in south- east of Angelele_ Fentale_ Dofen Magmatic Segment (MS) with increased b-value anomaly with lateral extension.

At a depth of 7 km (Fig. 11(c)), new features of the b-value anomalies appear beneath the Ankober boarder fault, Kone Ms. and south-east of Angelele_Fentale_ Dofen_MS and appeared to diminish. At depth 15 km (Fig. 11(d)), high b-value anomalies beneath Kone, south-east of Angelele_Fentale_Dofen_MS and Ankober boarder fault has not been seen, however a new high b-value anomaly in west of Ankober boarder fault was observed. With this, it may be concluded that seismic activity in the Ankober area is limited to 15 km depth only. In the (Fig. 11(a-d)),the horizontal and vertical black lines show the Ambo lineament and Ankober border Fault, respectively. The signature of high b-values beneath the faults and the lineaments is probably because of the high material heterogeneities and high crack densities, associated with high pore pressure and high temperature. NMER seismicity shows a concentration of medium to large -magnitude earthquake swarms at the base of (0.1–15) km deep seismogenic layer beneath the magmatic segments Fig. 11(e).

The major magmatic segments in CMER are shown in Fig. 12(f-i). These are Aluto MS, Aluto-Gedemsa_ MS and Boset-Kone_MS. The Guraghe boarder fault is also shown in CMER. Further, high b-value signatures are observed at a depth of 0.1 km beneath all the magmatic segments (see Fig. 12(f)) and Guraghe BF. Besides, no high b-value signature is observed beneath the Aluto_MS, however marginal b values are seen at this depth Fig. 12(f). At a depth of 7 km in Fig. 12(g) beneath all mentioned features except the Guraghe BF, high b-value anomaly of 1.3 is observed and these values correlate well with the works of Wilks et al. (2017) that they also obtained b-value of about 1.3 for the Aluto magmatic segment. This b -value might be a result of hydrothermal fluid from beneath the volcano of Aluto and dominantly normal faulting in the region (Wilks et al., 2017). High b-value anomaly starts to diminish from 7 km depth beneath the Guraghe BF which means that the Guraghe BF exists only up to a depth of 7 km for the period for which the catalogue was prepared under the present study (see Fig. 12(g and h)). Also, at a depth of 15 km all observed features, the Boset -Kone MS have increased in width and length and becomes continuous till this depth but it discontinued between 0.1 and 7 km slice depth (see Fig. 12(g and h)). The Guraghe BF is not observed well at this depth. Generally, other than features like Aluto, Boset-Kone_MS, and Guraghe BF, the rest regions have low b-value, probably indicating high stressed region.

The SMER average b-value, a-value and Mc respectively are 1.03 ± 0.1, 6.9 *and* 5.1 (see Fig. 14(c)).

High b-value signatures are observed throughout the depths of 0.1 km to 35 km and dipped in the South East-south west and north of SMER with high b-values (see Fig. 14(d and e)). The central part of SMER has relatively normal and low b-value near the volcano represented in the map. At 0.1 km depth, the high b-value is near and north of the volcano represented in the map. Further, It can be seen that strike along (SMER to Afar) the rift axis, beneath the NMER and Afar regions, relatively high signature of b-values exist, which indicate more active region (low stress region) and in the CMER it has low b-value anomaly which indicate low activity (high stress region).

Conclusions

A homogeneous earthquake catalog is of basic importance for studying the earthquake occurrence pattern in space and time. Such a catalog may also be useful for many engineering applications including assessment of seismic hazard, estimation of peak ground accelerations and determination of long-term seismic strain rates and seismic microzonation studies. Firstly, in this study, a homogenized earthquake catalog consists of 3814 moment magnitude Mw events for Ethiopia and adjoining region has been developed. This improved earthquake catalog of the country was prepared through systematic analysis to account for its completeness both in time and Magnitude.

Secondly, b-Values and maps were computed for Afar rift (including red sea and Gulf of Aden), Afar rift separately, Dabbahu volcano, NMER, CMER and SMER for the purpose of understanding the b-value characteristics of the regions. This implies the b-value can characterize the magma induced seismicity, magma chamber migration and movement in the study regions as confirmed by Fig. 9(a-d).

The seismicity parameters (average) a = 8.46 and b-value = 1.12 ± 0.02, magnitude of Completeness (Mc) = 4.6 and period of completeness from 2003 to 2015 are determined for Afar rift (including red sea and Gulf of Aden). Further, the average, a = 8.49 and b-value = 1.21 ± 0.04, magnitude of Completeness (Mc) = 4.8 and period of completeness from 2005 to 2014 are determined for Afar rift and Dabbahu Magmatic segment. Besides, the seismicity parameters (average) a = 5.77and b-value = 0.843, magnitude of Completeness (Mc) = 3.2 and period of completeness from 2001 to 2003 are determined for NMER. Similarly, a-value = 4.33and b-value = 0.826, magnitude of Completeness (Mc) = 3.1 and period of completeness from 2001 to 2003 are determined for CMER.

Finally, the seismicity parameters (average) a = 6.9and b-value = 1.03, magnitude of Completeness (Mc) = 5.1 and period of completeness from 1960 to 2016 are determined for SMER.

In general, the presence of magma gives rise to the main factors causing higher b-values, mainly high heterogeneity, and high thermal gradient in the study region. The presence of partial melt causes higher temperatures, in turn, a zone of relatively lower stress around the area of partial melt is created like in the case of Dabbahu volcano-magmatic segment and migration represented by high b-value signature (see Fig. 9(a-d)). It is observed beneath for some of the major magmatic segments in the rift and volcano are indicated by high b-values. Ankober Fault, Guraghe BF and Ambo lineaments are also indicated by high b-value anomaly. Magma chamber migration beneath the major volcanoes like Dabbahu, Angelele Fentale-Dofen etc. are parallelly indicated by elevated b-value anomaly. Hence, in this study, we clearly observed that magma chamber movement including mapping of volcanic centers and magmatic segments are mapped using b-values. Besides, Lineaments and faults can also be mapped using b-values.

Acknowledgements

Addis Ababa University financially supported this study. We also thank the Members Institute of Geophysics, Space and Astronomy (IGSSA) Addis Ababa University, provided us some seismicity data and kindly made discussions about the study.

Authors' contributions

GL Compiled and analyzed the earthquake data, graphical plotting's using MATLAB and other programs and was a major contributor in writing the manuscript. TM Technical Editing and write up of the manuscript. TKR Technical and language Editing and write up of the manuscript. All authors read and approved the final manuscript.

Funding

The sources of Funding and logistic works have been covered by Addis Ababa University, College of Natural Science through professor Tilahun Mammo.

Availability of data and materials

The datasets used and analyzed during the current study are available from the corresponding author on reasonable request. Some of the data generated during this study are included in this published article.

Ethics approval and consent to participate

Not applicable.

Consent for publication

Not applicable.

Competing interests

The authors declare that they have no competing interests.

Received: 15 December 2018 Accepted: 30 September 2019
Published online: 29 November 2019

References

Abbate, E., P. Bruni, and M. Sagri. 2015. *Geology of Ethiopia: A review and geomorphological perspectives world geomorphological landscapes book series (WGLC) landscapes*. Springer Science+Business Media Dordrecht 2015. https://doi.org/10.1007/978-94-017-8026-1_2 World Geomorphological Landscapes, DOI 10.1007/978-94-017-8026-1_2, © Springer Science+Business Media Dordrecht 2015. Ethiopian mapping authority, Ethiopia. doi: 10.5860/choice.192361.

Ahmed, A., Leroy, S., Keir, D., Korostelev, F., Khanbari, K., Rolandone, F., et al. (2014). Tectonophysics Crustal structure of the Gulf of Aden southern margi :

Evidence from receiver functions on Socotra Island (Yemen). Tectonophysics, 637, 251–267. https://doi.org/10.1016/j.tecto.2014.10.014
Aki, K. 1965. 'DETERMINING', maximum likelihood estimate of b in the formula log N= a-bM and its confidence limits. *Bulletin of the Earthquake Research Institute* 43: 237–239.
Aki, K. 1984. Asperities, barriers, characteristic earthquakes and strong motion prediction (Japan). *Journal of Geophysical Research* 89 (B7): 5867–5872. https://doi.org/10.1029/JB089iB07p05867.
Akkar, S., et al. 2010. The recently compiled Turkish strong motion database: Preliminary investigation for seismological parameters. *Journal of Seismology* 14 (3): 457–479. https://doi.org/10.1007/s10950-009-9176-9.
Alamilla, J.L., R. Vai, and L. Esteva. 2014. Completeness assessment of earthquake catalogues under uncertain knowledge. *Journal of Seismology* 19 (1): 27–40. https://doi.org/10.1007/s10950-014-9448-x.
Ayele, A. 1995. Earthquake catalogue of the horn of Africa for the period 1960–1993. *Seismological Department Seismological Department Uppsala, Report* 3–95: 1–9.
Ayele, A., et al. 2007. The august 2002 earthquake sequence in North Afar: Insights into the neotectonics of the Danakil microplate. *Journal of African Earth Sciences* 48 (2–3): 70–79. https://doi.org/10.1016/j.jafrearsci.2006.06.011.
Ayele, Atalay, and O. Kulhánek. 1997. Spatial and temporal variations of seismicity in the horn of Africa from 1960 to 1993. *Geophysical Journal International* 130: 805–810. https://doi.org/10.1111/j.1365-246X.1997.tb01875.x.
Ayele, Atalay, et al. 2015. Seismicity of the Central Afar rift and implications for Tendaho dam hazards. *Geological Society of London, Special Publication* 420 (1): 341–354. https://doi.org/10.1144/sp420.9.
Bastow, I. D., Stuart, G. W., Kendall, J.-M., & Ebinger, C. J. 2005. Upper-mantle seismic structure in a region of incipient continental breakup: northern Ethiopian rift, 162(2), 479–493. Retrieved November 8, 2019, from https://doi.org/10.1111/j.1365-246x.2005.02666.x.
Barberi, F., and J. Varet. 1977. Volcanism of Afar: Small-scale plate tectonics implications. *Bulletin Geological Society of America* 88 (9): 1251–1266. https://doi.org/10.1130/0016-7606(1977)88<1251:VOASPT>2.0.CO;2.
Bellahsen, N., et al. 2003. Why did Arabia separate from Africa? Insights from 3-D laboratory experiments. *Earth and Planetary Science Letters* 216 (3): 365–381. https://doi.org/10.1016/S0012-821X(03)00516-8.
Benoit, M.H., et al. 2003. Upper mantle P wave velocity structure and transition zone thickness beneath the Arabian shield. *Geophysical Research Letters* 30 (10). https://doi.org/10.1029/2002GL016436.
Benoit, B. 2006. La réalité selon Nietzsche, 131(4), 403. Retrieved November 8, 2019, from https://doi.org/10.3917/rphi.064.0403.
Bonini, M., Corti, G., Innocenti, F., Manetti, P., Mazzarini, F., Abebe, T., & Pecskay, Z. (2005). Evolution of the Main Ethiopian Rift in the frame of Afar and Kenya rifts propagation. Tectonics, 24(1), 1–21. https://doi.org/10.1029/2004TC001680.
Cauzzi, C., et al. 2016. Earthquake early warning and operational earthquake forecasting as real-time hazard information to mitigate seismic risk at nuclear facilities. *Bulletin of Earthquake Engineering* 14 (9): 2495–2512. https://doi.org/10.1007/s10518-016-9864-0.
Corti, G. 2009. Continental rift evolution: From rift initiation to incipient break-up in the Main Ethiopian rift, East Africa. *Earth-Science Reviews*Elsevier B.V 96 (1–2): 1–53. https://doi.org/10.1016/j.earscirev.2009.06.005.
Das, R. and Sharma, H. R. W. M. L. (2011) 'Global regression relations for conversion of surface wave and body wave magnitudes to moment magnitude'. doi: https://doi.org/10.1007/s11069-011-9796-6.
Data retrieved from the ISC web site. 2015. *International seismological Centre, on-line bulletin* http://www.isc.ac.uk. Thatcham: Internatl. Seismol. Cent.
Debayle, E., J.J. Lévêque, and M. Cara. 2001. Seismic evidence for a deeply rooted low-velocity anomaly in the upper mantle beneath the northeastern afro/Arabian continent. *Earth and Planetary Science Letters* 193 (3–4): 423–436. https://doi.org/10.1016/S0012-821X(01)00509-X.
Ebinger, C.J., and M. Casey. 2001. Continental breakup in magmatic provinces: An Ethiopian example. *Geology* 29 (6): 527–530. https://doi.org/10.1130/0091-7613(2001)029<0527:CBIMPA>2.0.CO;2.
Ebinger, C.J., et al. 2008. Capturing magma intrusion and faulting processes during continental rupture: Seismicity of the Dabbahu (Afar) rift. *Geophysical Journal International* 174 (3): 1138–1152. https://doi.org/10.1111/j.1365-246X.2008.03877.x.
Farrell, J., S. Husen, and R.B. Smith. 2009. Earthquake swarm and b-value characterization of the Yellowstone volcano-tectonic system. *Journal of Volcanology and Geothermal Research* 188 (1–3): 260–276. https://doi.org/10.1016/j.jvolgeores.2009.08.008.
Feng, M., et al. 2009. Depth and region dependence of b-value for micro-aftershocks of the may 12th, 2008 Wenchuan earthquake and its tectonic implications. *Earthquake Science* 22 (6): 589–594. https://doi.org/10.1007/s11589-009-0589-x.
Gardner, J.K., and L. Knopoff. 1974. Is the sequence of earthquakes in Southern California, with aftershocks removed, Poissonian? *Bulletin of the Seismological Society of America* 64 (5): 1363–1367 Available at: http://citeseerx.ist.psu.edu/viewdoc/download?doi=10.1.1.467.2509&rep=rep1&type=pdf.
Ghebreab, W. 1998. *Tectonics of the Red Sea region reassessed*.
Gouin, P. 1970. *'Gouin'. Phil. Trans. R. SOC. Lond*, 339–358.
Gouin, P. 1979. *Earthquake history of Ethiopia and the horn of Africa*. Ottawa: International Development Research Center.
Gutdeutsch, R., and C. Hammerl. 1999. *Journal of Seismology*, 3 (4): 351–362.
Hanks, T.C., and H. Kanamori. 1979. 'Fault mechanics', Journal of Geophysical Research, vol. 84, no. B5, p. 2145.
Hofstetter, R., and M. Beyth. 2003. The afar depression: Interpretation of the 1960–2000 earthquakes. *Geophysical Journal International* 155(2): 715–732. https://doi.org/10.1046/j.1365-246X.2003.02080.x.
Ishimoto, M., Iida, K, 1939. Observations of earthquakes registered with the microseismograph constructed recently, Bull. Earthq. Res. Inst. Univ. Tokyo, 17, 443–478.
Kadirioglu, F.T., and R.F. Kartal. 2016. The new empirical magnitude conversion relations using an improved earthquake catalogue for Turkey and its near vicinity (1900-2012). *Turkish Journal of Earth Sciences* 25 (4): 300–310. https://doi.org/10.3906/yer-1511-7.
Kanamori. (1974). Focal process of the great Chilean earthquake May 22, 1960. Seismological Laboratory, California Institute of Technology, Pasadena, Calif. U.S.A., 33(3), 371–386. https://doi.org/10.1016/0031-9201(74)90029–6.
Karimiparidari, S., et al. 2013. Iranian earthquakes, a uniform catalog with moment magnitudes. *Journal of Seismology* 17 (3): 897–911. https://doi.org/10.1007/s10950-013-9360-9.
Kebede, F., and L.M. Asfaw. 1996. Seismic Hazard assessment for Ethiopia and the neighboring countries. *Sinet – Ethiopian journal of science* 19 (1): 15–50 [34].
Kebede, Fekadu. 1996. Seismic Hazard Assessment for the Horn of Africa. *Journal of Ethiopian Engineers and Architects, Sinet* 1: 15–50.
Keir, D. 2006. *Strain Accommodation by Magmatism and Faulting as Rifting Proceeds to Breakup: Seismicity of the Northern Ethiopian Rift*. Royal Holloway University of London.
Manighetti, I., King, G. C. P., & Gaudemer, Y, kif, W. 2001. Water Volcanoes, 106.
Mogi, K. 1962. *'Mogi', magnitude-frequency relationship for elastic shocks accompanying fractures of various materials and some related problems in earthquakes*. Vol. 40, 831–853. Tokyo: Bulletin of the earthquake research institute, University of Tokyo.
Morley, C.K., et al. 2007. Tectonic evolution of the northern Kenyan rift. *Journal of the Geological Society* 149 (3): 333–348. https://doi.org/10.1144/gsjgs.149.3.0333.
Murru, M., et al. 2007. Spatial mapping of the b value at Mount Etna, Italy, using earthquake data recorded from 1999 to 2005. *Journal of Geophysical Research - Solid Earth* 112 (12). https://doi.org/10.1029/2006JB004791.
Nasir, A., et al. 2010. Assessing the completeness of historical earthquake records in Austria and surrounding Central Europe. *Austrian Journal of Earth Sciences* 12: 90–102.
Nuannin, P. 2006. *The potential of b -value variations as earthquake precursors for small and large events*.
Prasad, S., and C. Singh. 2015. Evolution of B-values before large earthquakes of m<inf>b</inf>≥6.0 in the andaman region. *Geologica Acta*: 205–210. https://doi.org/10.1344/GeologicaActa2015.13.3.3.
Reasenberg. 1985. Second-order moment of central California seismicity. 1969–82, J. Geophys. Res, 90, 3–18.
Rierola, M. 2005. *Temporal and spatial transients in b-values beneath volcanoes*. Zurich: ETH Zurich, Institute of Geophysics.
Samuel, K, Samson, E, Kebede, A, and Tessema E . 2011. Technical notes and proposed guidelines on updated seismic codes in ethiopia implication for large-scale infrastructures. *Journal of Ethiopian Engieers and Archtects (EEA)* 28: 92–110.
Scholz, C.H. 1968. The frequency-magnitude relation of microfracturing in rock and its relation to earthquakes. *Bulletin of the Seismological Society of America* 58 (1): 399–415 Available at: http://www.bssaonline.org/cgi/content/abstract/58/1/399.
Scordilis, E.M. 2006. Empirical global relations converting MS and mb to moment magnitude. *Journal of Seismology* 10 (2): 225–236. https://doi.org/10.1007/s10950-006-9012-4.
Shi, Y., and B.A. Bolt. 1982. The standard error of the magnitude-frequency b-value. *Bulletin of the Seismological Society of America* 72 (5): 1677–1687.
Singh, A.P., et al. 2015. Seismic source characteristics in Kachchh and Saurashtra regions of Western India: B-value and fractal dimension mapping of

aftershock sequences. *Natural Hazards* 77: S33–S49. https://doi.org/10.1007/s11069-013-1005-3.

Talukdar, Pulama. 2014. Preparation of a comprehensive earthquake catalog for Northeast India and its completeness analysis\n. *IOSR Journal of Applied Geology and Geophysics (IOSR-JAGG)*: 22–26 Available at: http://www.iosrjournals.org/iosr-jagg/papers/vol2-issue6/Version-1/D02612226.pdf.

Trebbin, N., and J. Wassermann. 2010. *Seismic data analysis with ObsPy*. Ludwig-Maximilians-University Munich.

Uhrhammer, R. 1986. Characteristics of Northern and Central California Seismicity, Earthquake Notes, 57(1): 21.

Vergne, A., Doubre, C., Leroy, S., Kassim, M., Keir, D., Abayazid, A., ... Al-Ganad, I. 2016. Seafloor spreading event in western Gulf of Aden during the November 2010-March 2011 period captured by regional seismic networks: Evidence for diking events and interactions with a nascent transform zone. Geophysical Journal International, 205(2), 1244–1266. https://doi.org/10.1093/gji/ggw068.

Wiemer, S. 2001. A software package to analyse seismicity: ZMAP. *Seismological Research Letters*: 373–382. https://doi.org/10.1785/gssrl.72.3.373.

Wiemer, S., and J.P. Benoit. 1996. Mapping the b-value anomaly at 100 km depth in the Alaska and New Zealand subduction zones. *Geophysical Research L* 23 (13): 1557–1560.

Wiemer, S., and M. Wyss. 1997. Mapping the frequency-magnitude distribution in asperities: An improved technique to calculate recurrence times? *Journal of Geophysical Research* 102 (3): 15115. https://doi.org/10.1029/97JB00726.

Wiemer, S., and M. Wyss. 2002. ZMAP -- A Tool for Analyses of Seismicity Patterns. Writing. Retrieved from https://www.seismo.ethz.ch/prod/software/zmap/index_EN.

Wilks, M., Kendall, J. M., Nowacki, A., Biggs, J., Wookey, J., Birhanu, Y., … Bedada, T. 2017. Seismicity associated with magmatism, faulting and hydrothermal circulation at Aluto Volcano, Main Ethiopian Rift. Journal of Volcanology and Geothermal Research, 340, 52–67. https://doi.org/10.1016/j.jvolgeores.2017.04.003.

Woessner, J., and S. Wiemer. 2005. Assessing the quality of earthquake catalogues : Estimating the magnitude of completeness and its uncertainty. *Bulletin of the Seismological Society of America* 95 (2): 684–698. https://doi.org/10.1785/0120040007.

Wyss, M. 1973. Towards a physical understanding of the earthquake frequency distribution. *Geophysical Journal of the Royal Astronomical Society* 31 (4): 341–359. https://doi.org/10.1111/j.1365-246X.1973.tb06506.x.

Wyss, M., S. Wiemer, and R. Zuniga. 2001. *ZMAP -- a tool for analyses of seismicity patterns, writing* Available at: http://www.seismo.ethz.ch/prod/software/zmap/index_EN.

Yirgu, G., A. Ababa, and A. Ayele. 2006. Recent seismovolcanic crisis in northern Afar, Ethiopia. *Eos, Transactions American* … 87 (33): 2–5. https://doi.org/10.1029/2006EO330001.

Publisher's Note